Finding the Roots of Microturbulence

Ilse Kuperus

Thesis submitted for the degree of
Master of Science in Astronomy

Institute of Theoretical Astrophysics
University of Oslo

12th May 2022

Copyright © 2021, Ilse Kuperus

This work, entitled “Finding the Roots of Microturbulence” is distributed under the terms of the Public Library of Science Open Access License, a copy of which can be found at http://www.publiclibraryofscience.org.

Abstract

The use of microturbulence as a free parameter is often done in stellar and solar astrophysics. This is a parameter that gets added when comparing the equivalent width of observations to the models when looking at stellar abundances (Mucciarelli 2011) or for the purpose of inversions (Socas-Navarro 2015). However, neither the value of this microturbulence nor the roots are universally agreed upon. For the photosphere 3D modelling has been shown to reduce or completely remove the need for microturbulence in the model (Asplund 2005), however in the chromosphere microturbulence is still added to both 1D and 3D models (da Silva Santos et al. 2020; Socas-Navarro 2015). The value of microturbulence and its roots are important as microturbulence is used to find values for physical parameters in the star or the abundance in the star. Therefore, finding the right microturbulence value or disregarding the microturbulence completely is of importance for the information we find.

We made one-dimensional optical depth averages ($\langle 3D \rangle_\tau$) by averaging a Bifrost 3D model, and added four different microturbulence recipes to this average. Then we compared Ca II 854.2 nm synthetic line profiles for these $\langle 3D \rangle$ models to the line profile from the 3D model. From this we found that although the equivalent width of the $\langle 3D \rangle$ model is closer to that of the 3D model when a microturbulence of $\frac{1}{3}\sqrt{v_x^2 + v_y^2 + v_z^2}$ is added, the shapes of the lines are not a good fit. Further, we have split the 3D atmospheres into smaller boxes to look more closely at the fit in different areas. The atmosphere is split into boxes of around $230\text{km} \times 230\text{km}$ and $1150\text{km} \times 1150\text{km}$ horizontally. We found that when looking at the smallest boxes microturbulence gives the $\langle 3D \rangle$ lines a worse fit, while in the larger boxes the the addition of microturbulence does not change the overall goodness of fit. When looking into the roots of the microturbulence, we found that there seems to be a weak correlation between the high temperature and velocity areas and the areas with a large difference in the line profile, but neither of these parameters is enough to explain the microturbulence on its own. Overall, the main difference between between the spectra from the 3D model and the $\langle 3D \rangle$ model comes from the averaging itself, and the addition of microturbulence reduces the difference on a larger scale, but not on a smaller scale. Therefore, we concluded that the microturbulence works as a smoothing parameter to compensate for 3D motions in the $\langle 3D \rangle$ model, but is not a physical parameter.

Acknowledgments

The biggest thank you to my supervisor, Tiago Pereira, for all the guidance when working on this project, for helping me refocus when I felt stuck and for helping me make sense of things. Thanks to ITA and RoCS for being such a nice place to study, for creating a good environment to learn and for allowing me to be a part of the research you do. Thanks to all my fellow astronomy students for being supportive, for being good collaborators, and for all the interesting conversations we had when we should have been working.

I also want to thank all my family and friends who have supported me all five years of my degree. Special thanks to my mother for encouraging me when I doubted myself and for proofreading my thesis. Lastly, thanks to Hans Einar for supporting me all the way, and for encouraging me to follow my dreams even when they seem too difficult.

Contents

Chapter 1

Introduction

It is common in solar and stellar astrophysics to use simulations and models of stars to learn more about the star because few physical quantities can be inferred from the observations alone. Such simulations are a very helpful tool to learn more about the Sun and are used frequently to determine how the Sun behaves and how the observations should be interpreted. A simulation will include the known processes in the Sun in order to recreate the solar atmosphere in the best way possible. From a simulation of the solar atmosphere, we can perform radiative transfer to synthesise spectral line profiles. Despite the stars being three-dimensional, atmosphere models are often made in one dimension because it is much less complicated and computationally less expensive than doing a three-dimensional line profile synthesis. When performing this synthesis in one dimension instead of three, we lose some information in simplifying the dimensions. To compensate for the loss of information there have been attempts to add additional parameters. One-dimensional models of the solar atmosphere lack a realistic treatment of convection; to make up for this in the line shape, microturbulence is added. Microturbulence is an artificial parameter added to account for Doppler motions from convection that are not present in one-dimensional stellar models, it is used to give broader spectral lines when fitting the model to the observations. Although we frequently see that this microturbulence parameter is added when using model atmospheres to gain information from the Sun or other stars, its cause and origin are unknown.

Both in stellar and solar physics microturbulence is used as a parameter when attempting to obtain information about the star, albeit in different ways. In stellar astrophysics finding the abundance of different elements is of importance to learn more about stars, to do this one-dimensional models are often used to get spectral lines which are fitted to the spectra from observations. Microturbulence is often used jointly with macroturbulence as a free parameter when making these models used for finding the abundances in the stars. The micro-and macroturbulences are adjusted to make the theoretical equivalent widths fit the lines, (e.g. Magain 1984; Mucciarelli 2011). The values of microturbulence used for these stars depend on the stars and the lines looked at. Edvardsson et al. (1993) determine abundances using one-dimensional models and use a constant microturbulence value of $0.3\,\mathrm{km\,s^{-1}}$ to fit the observed equivalent width

of the Fe I and Ni I lines. In solar astrophysics the microturbulence is also used in a different application. Here the microturbulence is used as a free parameter when performing inversions (see Ruiz Cobo & del Toro Iniesta 1992; Sainz Dalda et al. 2019). Inversions are done to find more information about the Sun. A model is made from which a spectrum can be obtained, this spectrum is then compared to observation. The model can be changed so that the model spectrum fits the observed spectrum, and then it is inverted to find the atmosphere values corresponding to the spectrum that best fits the observations. The physical properties of the Sun can be extracted from the model atmosphere found with inversions as seen in Beck et al. (2015). When changing the model so that the spectral line fits the observed line the microturbulence comes in as a parameter, this can be added and changed to adjust the width of the spectral line. In one-dimensional inversion models, the value of the microturbulence parameter in the chromosphere is sometimes determined to be as high as $6\,\mathrm{km\,s^{-1}}$ (da Silva Santos et al. 2020). When we instead use three-dimensional atmospheres to synthesise we will have a model that should more closely represent the real effects in the Sun, as 3D effects are included. For this to be possible we need to have a model that includes the most important processes in the Sun that will affect the spectral lines. It appears that with a better understanding of the stellar photosphere and better 3D models the microturbulence will possibly be obsolete (Asplund 2005). However, other studies using three-dimensional models will still use microturbulence in the inversion to make a better fit, we see this in Socas-Navarro (2015) where a microturbulence of $0.8\mathrm{kms^{-1}}$ is used for the Sc II line, but no microturbulence is used for the Fe I line, when looking at the abundance of oxygen in the Sun. It is also important to note that the microturbulence values found have been shown to depend on the angle. Takeda (2022) determine the microturbulence value from the disk centre through the limbs from the Fe I lines and find it to be different depending on the viewing angle, here the disk centre value of the microturbulence is $1\,\mathrm{km\,s^{-1}}$.

We can see that the use of microturbulence as a parameter in both stellar and solar physics is widely used, despite the values determined being different and the origin of this parameter unknown. Presently it is still common practice to use a one-dimensional model for inversions or abundances and add the additional microturbulence for broadening of the line. Asplund (2005) described the use of three-dimensional models has removed the need for additional microturbulence when looking at the photosphere. However since the chromosphere is a much more dynamic layer, it is has been more difficult to capture all processes with the current 3D modelling. The synthesis of chromospheric lines from three-dimensional models is more computationally expensive and thus one-dimensional models are still more widely used. In addition, the matter is organised on a smaller scale which we may not yet have the necessary spatial resolution to capture. These are both justifications used for why the spectral lines even from a 3D model are still narrower than the observation (see Leenaarts et al. 2009) and why it is therefore in many cases still deemed necessary to add microturbulence to the chromospheric lines from the model. In this project, we will attempt to get more information on the origins of microturbulence in the solar chromosphere by performing spectral synthesis of chromospheric lines. We will be using 3D simulations of the solar chromosphere and

comparing these to average models of the 3D simulation ($\langle 3D \rangle$) with added microturbulence. Using a $\langle 3D \rangle$ model has both advantages and drawbacks, both of which have been explored on several occasions (e.g. in Gustafsson et al. 2008)). Generally, $\langle 3D \rangle$ models have the advantage that they are much easier to simulate, they are much less complicated and require far less computational power than a 3D model does, but as we need to add the unknown microturbulence parameter these models are more difficult to interpret. The main goal of this project is to understand what causes microturbulence, whether it is a real parameter or a parameter that is added to compensate for unresolved motions. We will do this by finding the best microturbulence recipes for the chromosphere, comparing $\langle 3D \rangle$ models with these microturbulence parameters to the 3D model and looking at how and where these models differ. By analysing the microturbulence of the different models and exploring its relation to the other known parameters that affect the profiles we hope to find more information on what creates this microturbulence factor.

Chapter 2

Background

Models of the solar atmosphere are made to obtain line profiles. These line profiles can provide us with information that is difficult to gain from only looking at observations. For instance, values of the physical parameters in the Sun can be acquired by using a model and inversions. Since our goal is to find the roots of microturbulence in the solar chromosphere we need to make model atmospheres in three dimensions and one dimension from which we can get spectra. The spectra are made from numerical simulations of the atmosphere. From these simulations spectra can be made by use of radiative transfer calculations, and from these spectra, specific line profiles can be plotted. As the density and the temperature of the atmosphere change in the different layers of the solar atmosphere, spectral lines are formed in different layers. We want to focus on looking at the microturbulence in the chromosphere and need therefore to look at specific spectral lines that are formed in the chromosphere.

2.1 Radiative Transfer

To make a line profile plot for the model atmosphere we need to perform the radiative transfer calculations on this model. These calculations will allow us to calculate the intensity in the model atmosphere. The spectral line is a measure of the intensity at different wavelengths. So, to plot the spectral line we need to find how we can calculate the intensity. In this chapter, we will look at how to calculate the spectral lines from the simulated atmospheres. The theory on astrophysical radiative transfer in section 2.1 is based on information from Rutten (2003).

2.1.1 Transport Equation

The radiation in the Sun is made up of photons with different energies travelling in all different directions. To describe this radiation, we can use the intensity, I_ν. This can be defined in terms of the energy that is transported in the radiation field. Formally, it is quantified as the energy in a frequency band dν transported over a time interval dt

through the area dA, and over the solid angle dΩ.

$$I_\nu = \frac{\mathrm{dE}_\nu}{\mathrm{dt}\,\mathrm{d}\nu\,\mathrm{dA}\,\mathrm{d}\Omega}. \tag{2.1}$$

The intensity is given in the units $\mathrm{W\,m^{-2}\,Hz^{-1}\,sr^{-1}}$. It is this intensity that we want to calculate in order to determine the different spectral lines. The intensity changes throughout the atmosphere, and to find how it changes along a beam we need to know how much energy is added and removed from this beam. If nothing is added or removed along the beam the intensity is constant. For energy to be added or removed from a beam, there needs to be matter in the path of the light. Adding energy to the radiation field is called emission, photons are added to the beam from photon creation, scattering, or photon conversion. The emissivity, j_ν, is given in the units $\mathrm{W\,m^{-2}\,Hz^{-1}\,sr^{-1}}$. Just as the intensity, the emissivity depends on location, direction time, and frequency. The intensity added by a local photon emission to the beam with intensity I_ν over a path ds is,

$$\mathrm{dI}_\nu(\mathrm{s}) = \mathrm{j}_\nu(\mathrm{s})\,\mathrm{ds}. \tag{2.2}$$

Energy removed from the radiation field is extinction, the photons are removed from the beam through absorption (photon destruction), scattering, or photon conversion. The extinction is proportional to both the supply of photons and to the number of extinguishing particles, the proportionality coefficient, extinction coefficient, α_ν is given in the units $\mathrm{m^{-1}}$. The extinction per unit path length is,

$$\mathrm{dI}_\nu(\mathrm{s}) = -\alpha_\nu(\mathrm{s})\,\mathrm{I}_\nu(\mathrm{s})\,\mathrm{ds}. \tag{2.3}$$

This is identical to the extinction per unit volume. The extinction can also be expressed per particle by use of cross-section or per kilogram by use of mass density. If we use another definition the coefficient value will change. For simplicity, we will here only use the path per length definition of the extinction. If we combine the intensity change from emission in eq. (2.2) and extinction in eq. (2.3) to find the total change in intensity we obtain the equation,

$$\mathrm{dI}_\nu = \mathrm{j}_\nu(\mathrm{s})\,\mathrm{ds} - \alpha_\nu(\mathrm{s})\,\mathrm{I}_\nu(\mathrm{s})\,\mathrm{ds}, \tag{2.4}$$

which can be rewritten as,

$$\frac{\mathrm{dI}_\nu}{\mathrm{ds}} = j_\nu - \alpha_\nu I_\nu. \tag{2.5}$$

This is the transport equation. This is an equation that applies generally when the extinguishing particles are small with respect to the separation between them and are randomly distributed. So, to find the intensity for any given frequency we need to find the extinction and emission at each frequency.

Since the measure of intensity over a given path is found from the extinction and emission along this path it is beneficial to define a few more terms. One of the important terms in the radiative transfer is the optical depth. The optical depth, or monochromatic optical depth, τ_ν, is the extinction along the path in the direction against the beam.

It is defined with a negative sign because of the direction we calculate this parameter, from infinity, the observer, to the location inside the object we are looking at,

$$\tau_\nu(z_0) = -\int_\infty^{z_0} \alpha_\nu(z)\,\mathrm{dz}. \tag{2.6}$$

Another useful quantity to define is the source function, the source function is important because it is the ratio between the emissivity coefficient and the extinction coefficient

$$S_\nu = \frac{j_\nu}{\alpha_\nu}.$$

The source function has units W m^{-2} Hz^{-1} sr^{-1}, which are the same units as the intensity has, this is important because it means that the source function and the intensity can be added and subtracted from each other. The source function is a useful quantity because it quantifies the addition of new photons along the beam. When we use the source function and the optical path together we can express the transport equation in terms of these quantities,

$$\frac{\mathrm{dI}_\nu}{\mathrm{d}\tau_\nu} = S_\nu - I_\nu. \tag{2.7}$$

This equation describes the change in the intensity per unit optical path, where S_ν is the source term in the equation. If there is no addition of photons to the beam, $S_\nu = 0$, the intensity will simply decrease exponentially. However, when the source function is not zero this is the equation we have to solve to find the intensity along a beam for a given frequency.

$$I_\nu(D) = I_\nu(0)e^{-\tau_\nu(D)} + \int_0^{-\tau_\nu(D)} S_\nu(s)e^{-[\tau_\nu(D)-\tau_\nu(s)]}\ \mathrm{d}\tau_\nu(\mathrm{s}). \tag{2.8}$$

2.1.2 Spectral Line Formation

Spectral lines are the result of the bound-bound process in the atoms. A bound-bound process in an atom is when an electron moves from one discrete energy level in the atom to another. The electron can go from an energy lower level to a higher one by being excited, this can happen by collision, where the electron absorbs the kinetic energy created in a collision or by absorbing a photon. In excitation, there is energy removed from the beam. When moving from a higher energy level to a lower one we have de-excitation, this can also occur by collision or by photon radiation. The wavelength of the photons involved is determined by the difference in energy between the levels $\lambda = hc/\Delta E_{mn}$. It is thus the difference in energy between the levels that determines the wavelength of the spectral line, which is why we can determine from what atom and which transition a line comes. These bound-bound processes create line profiles by affecting the extinction and the emission we introduced, which will determine the intensity for each frequency.

The extinction, emission and source function we have in equation (2.8) can be split into the line and continuum components. The line components, α_ν^l, j_ν^l, S_ν^l are the

components that come from the contribution from bound-bound transition to the extinction, emission and source function. The continuum components, α_ν^c, j_ν^c, S_ν^c, are the contributions from the bound-free and the free-free processes. When we break them down into the components we get;

$$S_\nu = \frac{\alpha_\nu^l S_\nu^l + \alpha_\nu^c S_\nu^c}{\alpha_\nu^l + \alpha_\nu^c}, \tag{2.9}$$

$$\alpha_\nu = \alpha_\nu^l + \alpha_\nu^c, \tag{2.10}$$

$$j_\nu = j_\nu^l + j_\nu^c, \tag{2.11}$$

$$S_\nu^l = \frac{\alpha_\nu^l}{j_\nu^l}, \quad S_\nu^c = \frac{\alpha_\nu^c}{j_\nu^c}. \tag{2.12}$$

The line components are needed to calculate the spectral line. The line component of the extinction is given by,

$$\alpha_\nu^l = \frac{h\nu_0}{4\pi}\left[n_l B_{lu}\phi(\nu-\nu_0) - n_u B_{ul}\chi(\nu-\nu_0)\right], \tag{2.13}$$

where n_u and n_l are the populations of the upper and lower levels. B_{lu} and B_{ul} are Einstein coefficients. The Einstein coefficients give the rate of transitions. B_{lu} is an Einstein coefficient for excitation, where $B_{lu}\overline{J_{\nu_0}}$ is the number of radiative excitations per particle from state l to state u per second. Similarly, B_{ul} is the Einstein coefficient for de-excitation, and $B_{ul}\overline{J_{\nu_0}}$ is the number of radiative de-excitations per particle from state u to state l per second. $\phi(\nu-\nu_0)$ and $\chi(\nu-\nu_0)$ are the profile functions for the corresponding transitions, ν is the frequency and ν_0 is the central frequency of the profile functions. For the line emission we have,

$$j_\nu^l = \frac{h\nu_0}{4\pi} n_u A_{ul}\psi(\nu-\nu_0), \tag{2.14}$$

Here A_{ul} is the Einstein coefficient for the rate of spontaneous de-excitation from level u to level l and $\psi(\nu-\nu_0)$ is the profile for spontaneous de-excitation. The source function for the line thus becomes,

$$S_\nu^l = \frac{j_\nu^l}{\alpha_\nu^l} = \frac{n_u A_{ul}\psi(\nu-\nu_0)}{n_l B_{lu}\phi(\nu-\nu_0) - n_u B_{ul}\chi(\nu-\nu_0)}. \tag{2.15}$$

In this project, we choose to only use complete redistribution (CRD) to reduce computation time and complexity, and thus the profile functions are all the same, $\phi = \chi = \psi$. We will use CRD for this project because it is a good approximation for most spectral lines, the only exceptions are very strong lines. This profile function is the line profile determined by the broadening processes. The shape of the line is thus determined from the thermal broadening which gives the line a Gaussian shape, and the collisional and radiative dampening which gives a Lorentz shape. The combination of these shapes makes a Voigt function which has a Doppler core and Lorentzian wings.

$$H(a,v) = \frac{a}{\pi}\int_{-\infty}^{\infty} \frac{e^{-y}}{(v-y)^2\ a^2}\,\mathrm{dy}, \tag{2.16}$$

where a is the damping parameter given as,

$$a = \frac{\gamma}{4\pi\Delta\nu_D}, \tag{2.17}$$

v is,

$$v = \frac{\nu - \nu_0}{\Delta\nu_D}, \tag{2.18}$$

and y is,

$$y = \frac{v_{los}}{c}\frac{\nu_0}{\Delta\nu_D}, \tag{2.19}$$

where v_{los} is the line of sight velocity. $\Delta\nu_D$ is the Doppler width of the line. Doppler width is the thermal broadening of the line, but this is also where the artificial microturbulence parameter is added in an attempt to get a broader spectral line. The Doppler width can be written in terms of the frequency or the wavelength as,

$$\frac{\Delta\nu_D}{\nu_0} = \frac{\Delta\lambda_D}{\lambda_0} = \frac{1}{c}\sqrt{\frac{2kT}{m} + v_{turb}^2}, \tag{2.20}$$

where the first term in the square root is the thermal broadening and the second term is the microturbulence or the non-thermal broadening. The profile will then be,

$$\psi(\nu - \nu_0) = V(a, v) = \frac{H(a, v)}{\sqrt{\pi}\Delta\nu_D}. \tag{2.21}$$

It is in this profile in the line extinction and in the source function for the line, that we find the Doppler width in which we have this added non-thermal broadening or microturbulence. As we do not know what this factor is we will in this project be attempting to find the roots of this broadening, and estimating the best recipe for the microturbulence in the chromosphere in an attempt to learn more about the microturbulence.

2.1.3 LTE vs. NLTE

Local thermodynamic equilibrium (LTE) is a type of equilibrium condition that assumes that the matter is in equilibrium with the ambient kinetic temperature. In this condition, radiation may deviate from the temperature and the temperature may vary slowly through the medium. LTE is beneficial because it assumes that the Maxwell, Boltzmann and Saha laws hold and that the source function is equal to the Planck function,

$$B_\nu = \frac{2h\nu^3}{c^2}\frac{1}{e^{h\nu/kT} - 1}. \tag{2.22}$$

However, in contrast to thermodynamic equilibrium (TE) where the Planck function is also equal to the intensity, this is not the case in LTE. $S_\nu = B_\nu$, $B_\nu \neq I_\nu$, thus we can have spectral lines in LTE. The fundamental idea of LTE is that the radiation can escape the local area, but not the matter. The transfer of energy in the area is determined mostly by collisions. LTE is mainly present in dense, optically thick areas, such as in lower atmospheric layers such as the photosphere.

In higher layers of the atmosphere, the density decreases and radiation dominates over collision. Because of these characteristics in the higher layers, we can no longer assume that LTE holds. This means that the extinction coefficient may differ from that of LTE and the source function may differ from the Planck function. This area is much more difficult to describe; we know that LTE no longer is an assumption we can make therefore this area is usually called non-LTE or NLTE. Often, the LTE assumption is replaced with an assumption of statistical equilibrium, that the Maxwell distribution holds and that complete redistribution occurs. However, generally, NTLE only indicates that LTE no longer holds.

The chromosphere is a layer in the atmosphere of the Sun, it is around 3000 to 5000 km deep. It is above the photosphere and below the transition region. The chromosphere has a very low density, about ten thousand times less dense than the photosphere. In addition, the temperature in the chromosphere varies a great deal with height, first, it decreases with height, and then it climbs again. It is this strange temperature pattern and the low density that makes the chromosphere a harder layer to predict, and subsequently simulate, than the photosphere, (see Carlsson et al. 2019). For the lines that are formed in the chromosphere, we assume that these are NLTE lines because of the low density of the chromosphere. LTE is a good approximation of the lines formed in the photosphere.

2.1.4 Ca II 854.2 nm Line

When looking at the chromosphere of the Sun we need spectral lines that are sensitive to this layer. In Carlsson et al. (2019) we find information on the spectral lines which can be used for diagnostics in the chromosphere. In the optical and infrared, one finds several widely-used chromospheric lines such as the Ca II H and K lines, the Ca II infrared triplet, the Hα-line and the He I 1083- line. For the Ca II H and K lines partial redistribution (PRD) effects must be included to correctly model the lines, this will make the synthesis more difficult and computationally expensive, thus we will for this project not look at these lines. The Hα-line has a low atomic weight, due to this the thermal broadening is very large and makes this line a worse diagnostic for microturbulence (non-thermal broadening) than the other chromospheric lines are. The He I 1083- line, is also chromospheric, but this line is mostly visible in the active sun regions and is a better diagnostic for the magnetic field than for microturbulence. Thus, the lines we can look at are the Ca II infrared triplet. For this project we focus on the Ca II 854.2 nm line, this line is a good diagnostic line for the chromosphere with good magnetic sensitivity (Carlsson et al. 2019). The other two triplet lines are more difficult to use as diagnostics because they are troubled with blends. This line is commonly used for diagnostics in the chromosphere, (see Quintero Noda et al. 2016; de la Cruz Rodríguez et al. 2012).

2.2 Atmosphere Models

Simulated atmospheres are used to make models which in both stellar and solar astrophysics are used to make spectral lines which can be compared with observation and used to determine the processes in the star. Simulations make it possible to perform numerical experiments on model atmospheres to see how these changes affect the models and to map out what happens in the Sun. Spectral lines calculated from models and inversions are often used when finding abundances and values for physical parameters. To plot the spectral lines which we will use for diagnostics we first need to have a simulation of the atmosphere.

2.2.1 Bifrost Simulation

The simulated atmospheres we use in this project are both Bifrost simulation models. Bifrost is a numerical code that solves the magnetohydrodynamic equations on a staggered grid using a compact finite difference scheme. This code carries out a simulation of the Sun which produces a model that can be used for calculations. The Bifrost code is explained in detail in Gudiksen et al. (2011) and the simulations we use here are further explained in Moe et al. (2022). We use two snapshots taken at the same time with different resolutions, these snapshots are taken with a magnetic field configuration close to that of a coronal hole. These two snapshots are completely identical save for the spatial resolution used. The simulated atmosphere contains different atmosphere variables that are needed for further calculations. These variables include x, y, and z points, temperature, velocities, mass density and internal energy. Simulated atmospheres can also include more variables, but to find the microturbulence these are the only variables that are needed. In a three-dimensional atmosphere, the parameters are three-dimensional arrays. We will then use the parameters from this atmosphere file to make the calculations for the spectral lines.

We will be comparing different simulations to each other. Mainly, we will use a simulation of the same area of the sun with different resolutions. As mentioned, with the exception of the spatial resolution, these two atmospheres are identical. This is a $12\,\mathrm{Mm} \times 12\,\mathrm{Mm}$ area of the Sun in the horizontal directions. And a depth of about 10.5 Mm depth, which includes $-2.5\,\mathrm{Mm}$ under the surface and $8\,\mathrm{Mm}$ over the surface. Here the surface, $z = 0$, is defined where $\tau_{500} = 1$. We will be using two different resolutions for this project, the first one has a 23-km size pixel and the second has a 6-km size pixel. This means that the lower resolution atmosphere will have 512×512 pixels covering $12\,\mathrm{Mm} \times 12\,\mathrm{Mm}$, and the high-resolution atmosphere will have 2048×2048 pixels for the same size area. In both resolutions the pixels are distributed evenly in x- and y-direction. The depth of the atmospheres is not distributed evenly in pixels as they are in the horizontal directions, for both atmospheres the depth is fixed, but not constant. The 23-km resolution atmosphere has a 512-pixel depth. In the 6-km resolution atmosphere, we have 1024 pixels for the same physical depth. The depth points are placed more densely around the height of the photosphere and chromosphere and more sparsely around the height of the corona and the convection zone. For this simulation, we have

assumed periodic boundary conditions in x and y and open boundary conditions in z.

To get a quick view of how the resolutions change the atmosphere we can look at the disk centre intensity at the Ca II 854.2 nm line core.

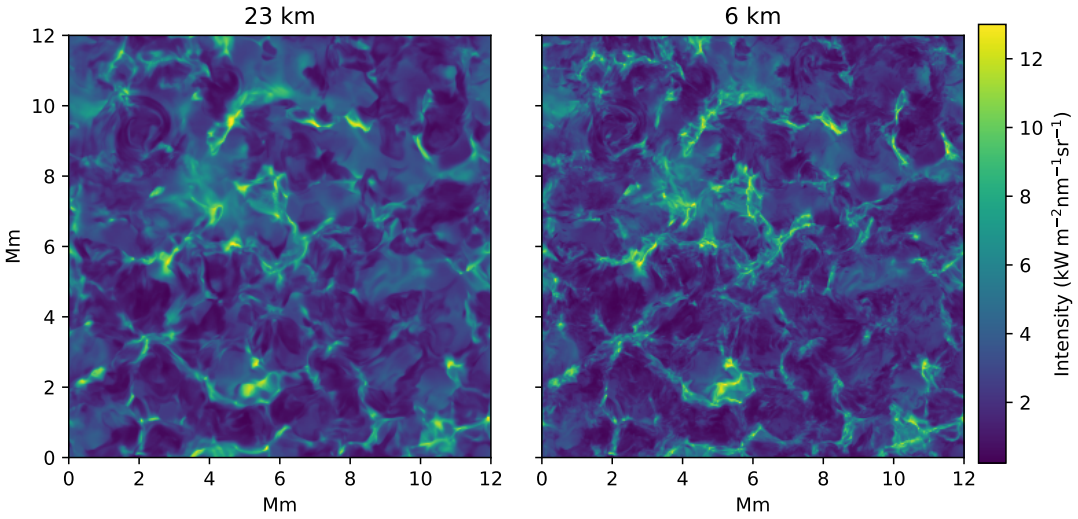

Figure 2.1: Disk-centre intensity maps of the Ca II 854.2 nm line core intensity. Maps for the same area of the sun with the two different resolution atmospheres we analyse in this project. The left image has a spatial resolution of 23 km per pixel and the right image has a spatial resolution of 6 km per pixel.

In Figure 2.1 we can see that the higher resolution atmosphere has more small details than the lower resolution atmosphere does. Since the higher resolution has more accurate detail it will be a better representation of the sun. These details in the intensity could potentially influence the spectral lines and the relation between microturbulence and the other parameters in the Sun.

2.2.2 Spectral Synthesis

To make the spectra from the simulations we need to perform spectral synthesis. The RH code is a radiative transfer code that synthesises spectra from stellar atmospheres. For this project we will be using the RH 1.5D code (Pereira & Uitenbroek 2015), which is a modification of the original RH code (Uitenbroek 2001), this 1.5D code can synthesise spectral lines from three-dimensional atmospheres column by column for it to be able to run parallel for large atmospheres. For the atmospheres, we use this RH 1.5D code to create the simulated line profiles, both for $\langle 3D \rangle$ models with microturbulence and 3D models. Since the Ca II 854.2 nm line does not suffer from strong 3D effects, the 1.5D is a good approximation. The RH 1.5D code will be used to calculate the intensity for a given atmosphere so that we can look at the spectral lines of this atmosphere.

2.2.3 Average Models

The use of one-dimensional averages ($\langle 3D \rangle$) is widespread. These averages can be made through the use of different methods, depending on how we make the averages and with respect to which parameters. Magic et al. (2013) explore different methods of making one-dimensional models and how these models compare to the spatially averaged spectral line of a full three-dimensional model for photospheric lines. They look at common averaging methods for $\langle 3D \rangle$ models of the Sun, these are some of the methods we will also use to look at the chromospheric line. The use of averages will change the spectral line and will be a simplification, this is arguably one of the reasons that the microturbulence parameter is needed, as this is an additional broadening that could account for motions that are three-dimensional and thus not present in these averages. Although there are downsides to making one-dimensional averages, such as the need for unknown parameters and simplifications, there are also benefits, such as faster computations and simpler models (Gustafsson et al. 2008). In many cases, one-dimensional models are used as they are simply the only option. Because the computation of a full 3D model will be too time-consuming to perform. Since a 3D model will contain more of the dynamics and interactions in the chromosphere we will compare the $\langle 3D \rangle$ model spectra we make to the 3D model spectrum.

Chapter 3

Methods

In this chapter, we will look at how we make spectra from the different model atmospheres. As mentioned we will make the spectra through the spectral synthesis in the RH 1.5D code. When we have a spectrum for the different model atmospheres, we will discuss how to find the ⟨3D⟩ averaging model that creates a line which best reproduces the line from the 3D model. Then, we will explore how to best look at different parts of the model atmosphere, and how to add microturbulence to the models. Finally, we explore how we want to attempt to find the roots of microturbulence. In this project we will refer to the roots of microturbulence, by this we mean finding the cause of the microturbulence or finding reasons for the addition of microturbulence to the models.

3.1 Averages of the 3D model

When creating the ⟨3D⟩ line profiles that we will be using we need to average the parameters from the 3D atmosphere file before synthesising the atmosphere using RH 1.5D. Taking the average of the 3D model before synthesis means that we don't have to do the RH calculations on all the columns, but rather on one column for each parameter, this makes the calculations less computationally expensive which is often a benefit to using ⟨3D⟩ models. The averaging of these parameters can be done in different ways, the way we choose to average the parameters will affect the parameters and thus the line profile we get from the model. To choose the averaging method we use in this case we compare geometrical height average, column mass average and an optical depth average at 500 nm. When comparing these averaging methods we will not be adding any microturbulence as the purpose is to choose which averaging method creates a line profile closest to the 3D line profile on its own. All of these averaging methods have been explored for the photosphere in Magic et al. (2013). For the comparison, we look at the Ca II 854.2 nm line. We decide which average is the one we will use based on which line is closest to the 3D line before adding any microturbulence, this average is then the one we will proceed with. To this average, we will then add values of microturbulence to make the ⟨3D⟩ model calcium line closer to the spatial average line of the full 3D spectrum.

The geometrical average in the height is found by taking the average over the x and y direction to get the average for each xy-plane.

$$\langle X \rangle_z = \frac{1}{N_x N_y} \sum_{i=0}^{N_x} \sum_{j=0}^{N_y} X_{ij,z}. \tag{3.1}$$

This is done for each parameter and will result in parameters that are one-dimensional and only vary with height. We will then have a geometrical average that has the same amount of points as the depth in the full 3D model. We do this for all parameters except for the z-velocity and the microturbulence for which we set all values to be zero, as we assume the average velocity to become zero and don't want any microturbulence at this stage. These averaged parameters are saved in an atmosphere file that is fed into RH for spectral synthesis.

For both the column mass average and the optical depth average, we need to interpolate and for this create new values for optical depth and column mass that are relevant for this line to use in the one-dimensional average. To find these values we want to start by looking at where this line is formed. We do this by using the parameter from RH 1.5D which gives the height at which each wavelength reaches an optical depth of one for each simulation column. By doing this we thus get one height value for each horizontal point and each wavelength, and by looking at a wavelength point for the core (854.2 nm) and one point for the wings (853.9 nm) of this line we can find the region of formation in height, optical depth and in column mass.

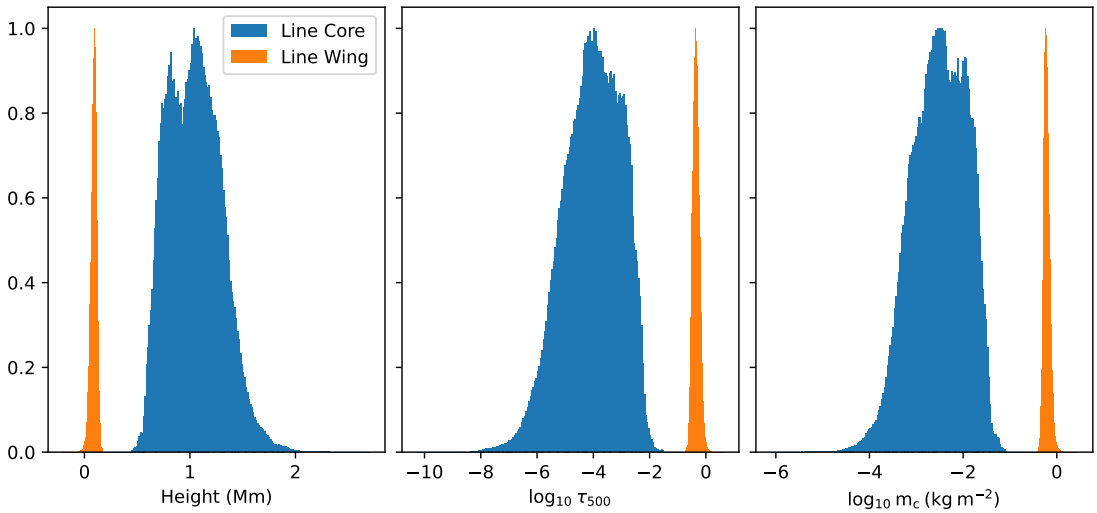

Figure 3.1: Region of formation for the Ca II 854.2 nm line, for wings and for line core.

In Figure 3.1 we see the region of formation for the line core and the line wing given in height, optical depth at 500 nm, and column mass. We see from this that the line core of Ca II 854.2 nm is formed in a region from around 0.5 Mm to 2 Mm and the wings are formed just above the surface. This corresponds to an optical depth at 500

nm region of formation of about $\log_{10}\tau_{500} = -8.0$ to $\log_{10}\tau_{500} = -2.5$ and column mass region from $\log_{10} m_c = -4.5$ to $\log_{10} m_c = -1.5$. When making the one-dimensional array for the interpolation we thus need to cover at least this line core formation region and the formation region of the wings.

To obtain the average over column mass we first need to find the column mass given the information we have from the simulation parameters. We integrate the mass density cumulatively for each column to get the column mass,

$$m_c = \int \rho \ \mathrm{dz}. \tag{3.2}$$

From this, we have a three-dimensional column mass density, which we can use for averaging. To make the column mass averages of the parameter we need to put these parameters on the column mass scale, which can be done with interpolation. To interpolate the different values to be on the column mass scale we need to set a one-dimensional column mass scale, we set this to be from $\log_{10} m_c = -6.0$ to $\log_{10} m_c = 2.0$ spaced linearly with the same number of points as the depth points in the three-dimensional column mass. These values will make sure we cover the formation of Ca II 854.2 nm. Then we interpolate the different variables over the z-axis with respect to the logarithm of the column mass $\log_{10} m_c$ and find new values using the new column mass. From this we have obtained the variables on a new depth scale, we average over iso-surfaces of constant column mass. Again the z-velocity and the microturbulence are set to zero. These values are all then used for the RH 1.5D calculations.

For the optical depth average we use the extinction at 500 nm from the RH 1.5D calculation of the 3D model, α_{500}, which can be integrated to get the optical depth, τ_{500}.

$$\tau_{500} = \int \alpha_{500} \, \mathrm{dz}. \tag{3.3}$$

This τ_{500} will then be a three-dimensional array with values for each column and each height. To find the average with respect to this optical depth we interpolate the different parameters with $\log_{10}\tau_{500}$ to get a new depth scale. For this interpolation, we need a new $\log_{10}\tau_{500}$ which is one dimensional to find the new values of the parameters. This new optical depth is set to go from $\log_{10}\tau_{500} = -8.0$ to $\log_{10}\tau_{500} = 4.0$ spaced linearly with the same number of points as the depth in the original scale. Just like in the column mass we have made this new optical depth to cover the formation of the Ca II 854.2 nm line. Now that we have interpolated and made new parameters that use the optical depth as height scale we can average over iso-surfaces of constant optical depth and create one-dimensional arrays. Similarly to column mass and geometric average we set microturbulence and z-velocity to be zero. When we create the average models we will not include the line of sight velocity in the average, this is because when we take an average we expect the line of sight velocity to cancel and the average to be zero.

We will thus use all these averaging methods to make new atmosphere models from which we calculate the intensity by using the RH code and make spectra. From this, we will look at which of these averaging methods gives a line profile closest to the 3D model spatially averaged line, and decide which averaging method we will proceed with.

Then we will add microturbulence to this average and make different models with added microturbulence values.

3.2 Smaller Boxes in the Atmosphere

As mentioned, we will be looking at the same simulated atmosphere with two different resolutions, 23-km resolution and 6-km resolution. The higher resolution will result in much more expensive computations, but the higher resolution allows for the detection of possible smaller-scale motions that could contribute to microturbulence. For these simulated atmospheres we will look at the line profiles of the Ca II 854.2 nm line, both for a spatial average of the 3D intensity and the intensity from the average models. For the full simulated atmosphere, we can get one 3D spectrum and one $\langle 3D \rangle$ spectrum for each recipe of microturbulence. For a more in-depth view of the atmosphere, it might be beneficial to split the atmosphere into smaller boxes. By doing this we will have atmosphere models for smaller parts of the atmosphere so that we can look at these smaller boxes and potentially get insight into how different parts of the atmosphere are averaged. This will also allow us to see how the addition of microturbulence to the model changes the line when we only look at a small atmosphere area. The splitting of the atmospheres into smaller boxes will hopefully allow us to gain more information on both the fit of the averaged line to the 3D line and the effect microturbulence has when adding it in a smaller scale model of the atmosphere. How microturbulence affects the line might change when looking at smaller boxes of the atmosphere as the spectra will not be smoothed over a large area and the smaller motions will to a larger degree affect the spectra.

We make the smaller atmosphere models by splitting the parameters in the simulated atmospheres into smaller boxes. All the boxes will have the same size and the boxes are roughly the same size in both atmosphere resolutions. For simplicity we have chosen to make 10×10 pixel and 50×50 pixel boxes for the 23-km resolution atmosphere, this translates to a physical size of 230 km $\times$ 230 km and 1150 km $\times$ 1150 km respectively. We have chosen 230km boxes because we wanted a very small box, but one that still contained enough pixels to have good statistics. The 1150km boxes are chosen to be around the size of a small granule. For the 6-km resolution we will then need boxes of 38×38 pixels and 192×192 pixels to keep approximately the same size, these will then be 228 km $\times$ 228 km and 1152 km $\times$ 1152 km. Each one of these smaller boxes will be synthesised by using RH 1.5D in the same manner as the full atmosphere, the smaller boxes will simply lead to many small atmospheres that are synthesised separately. For the smallest boxes, this means we have 2601 and 2809 atmosphere boxes respectively for the low and high resolutions, for all these individual small atmospheres the $\langle 3D \rangle$ needs to be calculated and the microturbulence recipes added. For the larger boxes, there are 100 atmosphere boxes in both resolutions, all of these also need individual $\langle 3D \rangle$ models and the addition of microturbulence. As the small boxes are smaller than the general size of a granule in the Sun, we expect there to be less motion in these boxes than in the whole atmosphere. The larger boxes are around the size of a granule, but

as they are not placed to fit the granules they will most likely contain parts of a granule in addition to inter-granule lanes. This means that these boxes will have more motions between sections, but give a more detailed view than an averaged model of the whole atmosphere can. When we split the atmosphere into smaller boxes and look at the line profiles we will include the line of sight velocity in the average unlike when we average the whole atmosphere, this is because we don't expect the velocity to average to zero when we look at only a small part of the atmosphere and thus the velocity is important to include.

By splitting the simulated atmosphere into sections we can look more closely at how the line profile changes in the atmosphere. These smaller boxes will hopefully allow us a more in-depth view of the relation between the lines and the physical variables that affect the shape of the line profile. In addition, these boxes allow us to make a map of the differences in the 3D line and the $\langle 3D \rangle$ lines, meaning that we can see in which of the boxes there is a large difference and in which the difference is small. This is helpful when looking at how well the $\langle 3D \rangle$ spectra compare to the 3D spectra. By looking at which boxes have a larger difference we can see how the physical parameters in these boxes correlate to this difference. It can also be used to compare the different $\langle 3D \rangle$ models when microturbulence is added by seeing if the addition of microturbulence changes which boxes have a high difference and if the overall difference diminishes. Such a map will be beneficial when we want to determine the roots of the microturbulence and when determining both if the $\langle 3D \rangle$ model is a good line profile estimation to the 3D model line and if the addition of microturbulence to the $\langle 3D \rangle$ improves the line profile.

3.3 Microturbulence

As we now have the spectral lines from the full 3D model and from the $\langle 3D \rangle$ model we want to see if we can add a microturbulence parameter to the $\langle 3D \rangle$ model which will improve the line profile from this $\langle 3D \rangle$ model compared to the line profile from the 3D model. We do this by adding microturbulence to the model before running RH to perform the spectral synthesis. Finding microturbulence parameters that can improve the line or that have been in previous papers in an attempt to improve the spectra is imperative to potentially finding the roots of microturbulence.

3.3.1 Adding microturbulence

To find the amount of microturbulence needed in this model of the atmosphere we add microturbulence to the $\langle 3D \rangle$ model and look at the difference between the line profiles from the $\langle 3D \rangle$ model and the 3D model. Since microturbulence has been added to one-dimensional models to compensate for the lack of broadening in the line we will need to find microturbulence values that broaden the line sufficiently. The value for the microturbulence can be found in many different ways from the atmosphere (examples of which can be found in Steffen et al. 2009). To attempt to find the roots of microturbulence we will add different values and then observe how these added values connect with existing variables in the atmosphere. We will compare four different recipes

for microturbulence, one where the microturbulence is 0km s^{-1} everywhere, one constant over height value, 2.15 km s^{-1}. This value is found by trial and error, picking the microturbulence value that gives the lowest difference in equivalent width between the $\langle 3D \rangle$ and the 3D line for the Ca II 854.2 nm line. The next microturbulence parameter we use is the standard deviation of the velocity in the z-direction, std(v_z), lastly, we will add a microturbulence recipe suggested by Uitenbroek & Criscuoli (2011),

$$v_{turb} = \frac{1}{3}\sqrt{v_x^2 + v_y^2 + v_z^2}. \tag{3.4}$$

In earlier research, the microturbulence value added is often assumed to be independent of height and constant. We see for Ca II 854.2 line the value found previously is 3 km s^{-1} (Quintero Noda et al. 2016; de la Cruz Rodríguez et al. 2012) which is close to the constant value of 2.15 km s^{-1} we implement. However, we also want to look at microturbulence recipes that change with height. Both std(v_z) and v_{turb} from eq. (3.4) will change with height as these both depend on velocity, which changes with height. We can see how these microturbulence values differ by plotting them with the height in the atmosphere.

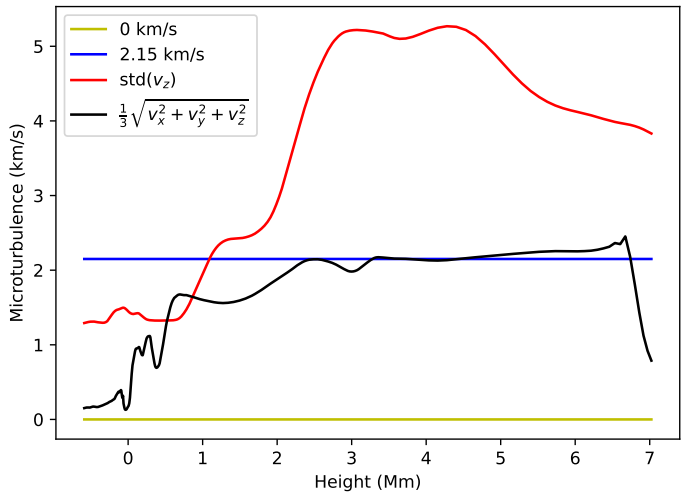

Figure 3.2: Microturbulence change with height for the different microturbulence recipes we will add to $\langle 3D \rangle$ model. 23-km pixel resolution atmosphere model.

Figure 3.2, shows how the microturbulence changes with height for the 23-km resolution atmosphere. We see that the constant value of 2.15 km s^{-1} has a good correlation with the microturbulence parameter given in eq. (3.4) in higher parts of the atmosphere, however, in the chromosphere, we have a steep increase in the values from both the microturbulence parameter given from std(v_z) and the parameter from v_{turb} (eq. (3.4)). This means that in the region where the line core for Ca II 854.2 is formed all the microturbulence additions are quite different. For the higher resolution atmosphere, the values are slightly different as the velocity values differ with a change in resolution, but the general trend is the same for the different microturbulence recipes.

3.3.2 Comparing Microturbulence

When comparing the different microturbulence recipes to each other and seeing which one will give a spectral line closer to the 3D model spectral line we need to quantify how good the fit is. For this, we will use both equivalent width, W, and what we will call the goodness of fit, Γ. The equivalent width calculates the area of the spectral line by integration,

$$W = \int I_\lambda - I_\lambda^c \, \mathrm{d}\lambda, \tag{3.5}$$

where I_λ^c is the continuum intensity and I_λ is the line intensity. We can then use this to compare the equivalent width of the 3D line to the equivalent width that we get from the $\langle 3\mathrm{D} \rangle$ spectral line with the different added microturbulence parameters. W will tell us if the lines have the same area and thus give us information on how similar the lines are.

The equivalent width is not a very good measurement if the shape of the lines is different as it is only a measurement of the area of the line. In addition, it is also not a good measurement if the line also includes some emission, because the line can then be more irregular which makes the area a less precise measurement. Therefore, we will use the goodness of fit, Γ, when we are looking at smaller areas of the atmosphere as these lines are generally more likely to be irregular. The goodness of fit will be defined as the difference in the intensity between the 3D model and the $\langle 3\mathrm{D} \rangle$ models with added microturbulence. The intensity is summed for each wavelength value so that we get one value for the goodness of fit.

$$\Gamma = \sum_\lambda \left(I_\lambda^{3\mathrm{D}} - I_\lambda^{\langle 3\mathrm{D} \rangle} \right)^2, \tag{3.6}$$

here $I_\lambda^{3\mathrm{D}}$ is the spatially-averaged intensity from the 3D model and $I_\lambda^{\langle 3\mathrm{D} \rangle}$ is the intensity from the $\langle 3\mathrm{D} \rangle$ model. Henceforth, when referring to the intensity from the 3D model we will be referring to the spatially-averaged intensity. This measure is what we use when we look at how well the $\langle 3\mathrm{D} \rangle$ line with microturbulence will estimate the 3D line when looking at the smaller boxes in the atmospheres. The Γ value gives us information on how large the difference in intensity between the models is, a high Γ value is a high difference and thus a bad fit while a low Γ is a low intensity difference and a good fit.

3.4 Roots of Microturbulence

Now that we have averaging methods, the microturbulence parameters to add and comparison methods, we expect to know more about how the microturbulence adds to the one-dimensional model and where it is lacking. From this, we aim to attempt to find the roots of microturbulence. For this project, we are using the expression finding the roots of microturbulence to mean finding what causes microturbulence or possible reasons for what the microturbulence is or how it is related to other parameters. We do this by comparing the value for Γ we get from calculating the goodness of fit to some of

the parameters in the Sun to see if there are any correlations between these parameters and Γ. For this we use the boxes of the atmosphere, we use these smaller boxes because we will then have a different Γ value for different parts of the atmosphere. Using this we will have a map for the atmospheres that tells us in which areas of the atmosphere the $\langle 3D \rangle$ line profile is a good approximation to the 3D line profile and which areas the $\langle 3D \rangle$ line is a bad fit. Since we have different microturbulence recipes that we have added to the average models we will also have Γ value maps for each of the $\langle 3D \rangle$ models, where each microturbulence recipe gives a separate model atmosphere. We will thus have four different Γ maps in each of the atmosphere splits, meaning that we in total have 16 Γ maps which give us information, 4 models for each box size, two box sizes and two different resolutions. Since we also look at the line from the model without any microturbulence we will have a Γ map which tells us where the averaging method is a good and bad fit when we have no additional microturbulence factor. This map will thus show the difference in the intensity between a 3D model and a $\langle 3D \rangle$ model and will be an indication of where the averaging method is lacking. We use this to determine where the Γ is high from the averaging methods and to compare to the other goodness of fit maps to see how the addition of microturbulence changes the $\langle 3D \rangle$ model. It is in these maps and the difference in the models with added microturbulence that we hope to find an indication of the roots of the microturbulence and gain more information on how this affects the model and in turn its place in the solar atmosphere.

To compare the $\langle 3D \rangle$ models with the 3D model we need to start by looking at the Γ values for the $\langle 3D \rangle$ model without any added microturbulence. We do this first as this will show the initial difference from just the averaging method. As this model is also one dimensional and thus a simplification we expect there to be a difference in the line profile between the $\langle 3D \rangle$ model and the 3D spatial averaged model. These Γ values will tell us something about the fit we get when we average the model and how this makes assumptions that are not necessarily correct. To look at where these averaging differences are coming from we can look at how the individual parameters are averaged. Since we have split the atmosphere into smaller boxes to obtain these Γ maps we will have one parameter value for each height for the average and multiple columns that we average in the 3D model, the number of columns depends on the size of the box and will be equal to the number of pixels in each box. So, if we have a 10x10 pixel box we have 10x10 columns in the 3D model that we average and one parameter column in the $\langle 3D \rangle$ model. To look at how the $\langle 3D \rangle$ model measures up in the parameter averaging we can plot all the individual columns from the 3D model with the single column for the $\langle 3D \rangle$ model, from this we will be able to see how the average of the parameter compares to all the columns of the same parameter. If we do this for one of the boxes that has a low Γ value and one box that has a high Γ value we can attempt to compare the averaging of different parameters to the goodness of the fit. Since all the parameters are averaged in the same way whether we add microturbulence or not this method will only tell us where the difference in the averaging method comes from. Assuming that the goodness of fit maps will look different if we add microturbulence we want to look at how the addition of microturbulence affects Γ.

Now that we have seen how we can compare the averaging of the parameters in

areas with a good and bad fit, we want to look at the Γ map as a whole. We want to explore if there is a correlation between the Γ maps and the parameters when we plot the parameters at the height where the Ca II 854.2 nm line is formed. We do this by plotting the parameters and seeing if there is correspondence with any of the parameters and the Γ values, for instance, whether the temperature is high or low or the z-velocity is high or low corresponds to the areas that have high or low Γ values. In addition to looking at the plain values of temperature and line of sight velocity we also want to look at a factor for the homogeneity of these variables. This is because a one-dimensional average of a three-dimensional atmosphere will have difficulty properly representing a large spread in values of a variable as it will only have the average and not include any of the extreme values. If there is a large spread the $\langle 3D \rangle$ model can thus give a line that has a large Γ because the model is too simple to represent the atmosphere. To look for such homogeneity we use the standard deviation of the variables for each smaller box, if we have a high standard deviation in one box it is more in-homogeneous. By looking at both the variables themselves and the homogeneity we attempt to say something about where the difference between the 3D model and the $\langle 3D \rangle$ model comes from, and whether the microturbulence will fix this or if it is just a shortcoming from other variables that have been too simplified in the averaging process.

Chapter 4

Results

In this chapter, we will explore the results we have obtained from the different microturbulence additions to the $\langle 3D \rangle$ models. Firstly, we start by looking at the results for which averaging method is best for this atmosphere and this line. Secondly, we look at how the addition of microturbulence changes the line profile and how it affects the overall difference of the line compared to the 3D model line. Finally, we look at the possible roots of this difference and how microturbulence can potentially be explained by looking at this difference.

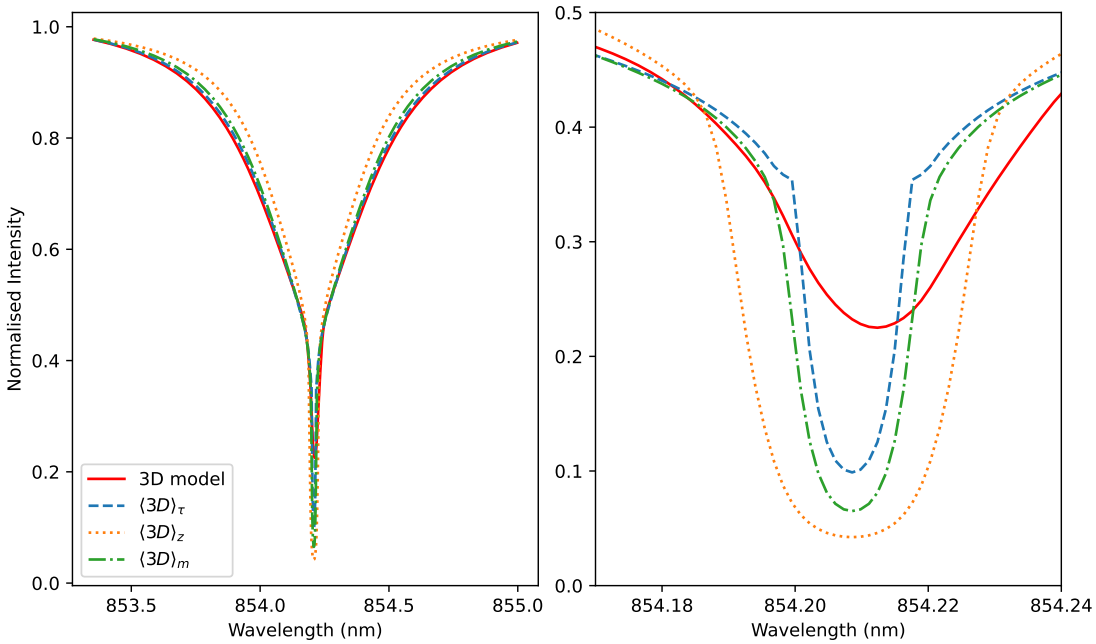

Figure 4.1: Line profile for the Ca II 854.2 nm line for both 3D model spatial average and optical depth at 500 nm ($\langle 3D \rangle_\tau$), column mass ($\langle 3D \rangle_m$) and geometrical average ($\langle 3D \rangle_z$) models. Left: full line profiles. Right: zoomed-in one line core.

4.1 Averages of the 3D model

There are multiple different ways to average a three-dimensional model to make a $\langle 3D \rangle$ model. For this project, we have done so by taking the geometric average, column mass average and the optical depth average to see which one gives a line profile closest to the 3D model spatial average line profile. When looking at the results of the intensity calculations of the three different one-dimensional averages of the 3D model we look at the Ca II 854.2 nm line.

In Figure 4.1, we see the line profile for the spatially averaged intensity calculated from the 3D model and the line profiles from the three different average models. As is the convention when looking at the averages there is no added z-velocity to the averages, therefore the line core of the 3D model line is shifted slightly in comparison to the lines from the $\langle 3D \rangle$ models. From this figure, we see that all of the averaging methods give line profiles that differ from the 3D model line, both in the wings and in the line core. The averages all have a line core that is deeper than the line core from the 3D model, this is an important thing to note as the addition of microturbulence does not change the line strength. In the wings we see that the 3D model line is stronger than the $\langle 3D \rangle$ model lines, here we also see that there is a large difference between the $\langle 3D \rangle$ model lines. From this figure, it seems that the line from the optical depth average model is closest to the 3D model line both in the line wings and in the line core. From these results, we thus decide that optical depth is the averaging method we will use when adding microturbulence to the average model. Thus, from now on, when the $\langle 3D \rangle$ is mentioned this will be referring to the optical depth average at 500 nm.

In order to explain the differences in the line profiles based on the averaging method we can look at properties of the model atmosphere. One of the important things in the Sun, especially in the chromosphere is the temperature at a given height. To illustrate the temperature at different heights for the 3D model we have used a probability density function (PDF), which shows which log temperatures are most likely at a given height. For the averages we plot a line of $\log_{10} T$ vs height. Figure 4.2 shows the log of temperature at each height. The PDF is normalized in such a way that for each height bin the temperature probabilities will sum to one, the darker temperatures are the most likely and the lighter ones are the less likely temperatures. Over this PDF we have plotted the temperature as a function of height for the three averaging methods. We notice in this figure that all three of the averages lay within the probability of the whole model, this means that they all fall within possible temperature regions. The wings for the Ca II 854.2 nm line are formed close to the surface of the Sun, and the core is formed in a region from about 0.5Mm to 1.5Mm, as we saw in the histograms in Figure 3.1. Thus we look at this region mainly when considering the averaging methods. Around the surface the temperature in the optical depth average is slightly lower than in the other averages which might explain why this line is closer to the 3D spatial average line in the wings than the other averages as we see that the PDF is darker at a lower temperature. However, in the region between 0.5 Mm and 2.0 Mm the $\langle 3D \rangle_\tau$ separates from the other two averages and has a higher temperature, this can explain why the optical depth average is more narrow in the line core than the other two averaging methods as

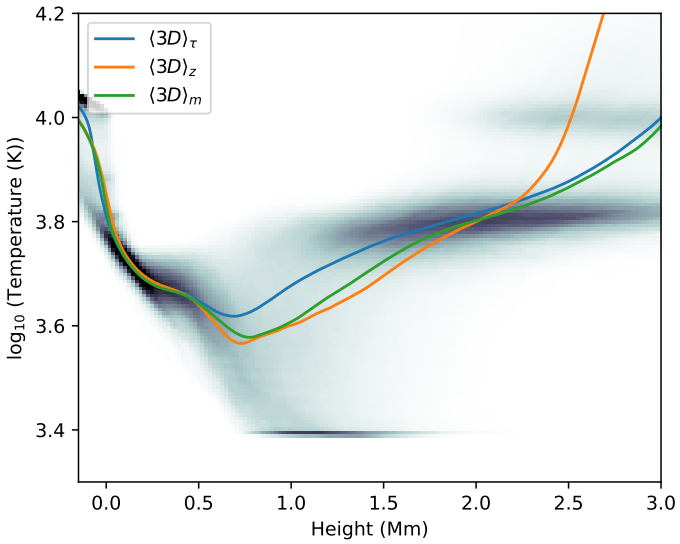

Figure 4.2: $\log_{10} T$ as a function of height for all three different averaging methods. See how the temperature changes depending on averaging method.

the temperature influences the Doppler width.

It is important to note that we decide to use the optical depth at 500 nm as the averaging method based on limited information. This averaging method gives the best result when comparing it to the geometrical and column mass averages for this particular line. This is the line we are using because this is a chromospheric line and we are looking in particular at how the microturbulence acts in the chromosphere. However, a different average may be better for other lines. It is also possible that there is another average that will fit the line better, but having looked at common averaging methods this is the averaging method that we will be continuing with. Magic et al. (2013) conclude that for the photospheric lines the $\langle 3D \rangle_m$ is the best averaging method, but also find that the line from $\langle 3D \rangle_\tau$ is a better fit to the 3D model line than the $\langle 3D \rangle_z$ line. In this mentioned paper, they look at lines from the photosphere in LTE while we look at NLTE lines, the different layers of the atmosphere might explain the difference in the best averaging method.

4.2 Different Microturbulence Recipes

4.2.1 Full Atmosphere

Having seen that the optical depth average is the best averaging method, this is the average we add microturbulence to in an attempt to get the $\langle 3D \rangle$ line close to the 3D model line. So, we have added the different microturbulence recipes to the $\langle 3D \rangle$ model and have performed the radiative transfer synthesis. By looking at the spectral line of the chromospheric calcium line we can then see the effect the addition of microturbulence has on the spectral line and compare it to the 3D model spectral line. We do this for the different atmospheres since we want to see if the resolution also contributes to the need for microturbulence. Firstly, we look at the line profiles and compare them by

looking at the equivalent width value, W. Starting by looking at the 854.2 nm Ca II line for model atmosphere at 23-km per pixel resolution.

Figure 4.3 shows the calcium line for the atmosphere with the 23-km resolution. We see from this figure both the full line and an image concentrated on the line core. In the left image of the figure we see that in the wings the 3D model line is lower than all of the average model lines, the right image shows that the average models all create lines with a stronger line core than the 3D model does. The strength of the line is not affected by the change in microturbulence so this difference in strength between the 3D line and the $\langle 3D \rangle$ lines will not be improved with added microturbulence. However, the width is the factor that changes when we add microturbulence. We can get a better understanding of how well the one-dimensional model lines compare to the three-dimensional model line we look at the equivalent width of the different lines in Table 4.1.

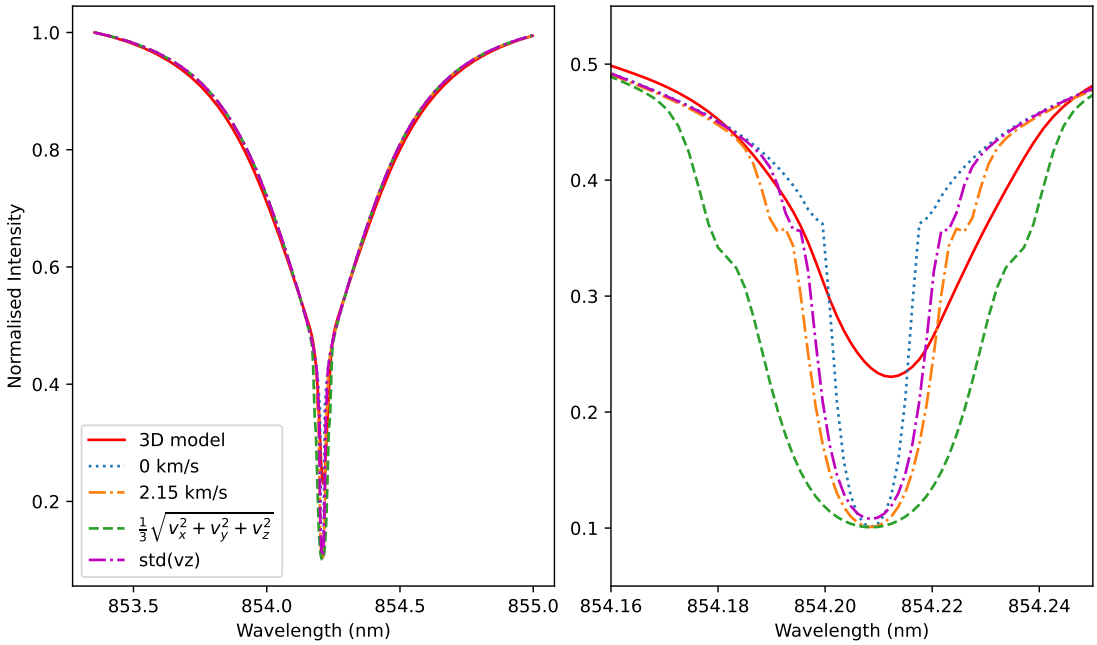

Figure 4.3: Ca II 854.2 nm disk-centre intensity for the 23-km resolution simulation. Left: full profile. Right: zoomed-in on line core

When looking at the lines they don't seem to fit very well with the 3D model, but when looking at the absolute difference between the equivalent width values the best fitting average model only has an absolute difference of +0.66%. It seems that the equivalent width is close despite the shape of the line core being different due to the small discrepancy in the wings. The 3D model line is stronger than the $\langle 3D \rangle$ model lines in the wings and it is compensated by being weaker than the $\langle 3D \rangle$ in the core. Thus, we have a line profile for the $\langle 3D \rangle$ model with added microturbulence which is a good fit when comparing the equivalent width values, but is not a good fit to the 3D model line in shape.

Line Profile	W (nm)	Deviation from 3D model
3D spatial average	0.298	—
0 km/s	0.290	−2.66%
2.15 km/s	0.293	−1.54%
$\frac{1}{3}\sqrt{v_x^2+v_y^2+v_z^2}$	0.299	+0.66%
std(v_z)	0.292	−2.05%

Table 4.1: Ca II 854.2 nm equivalent widths for 3D model line and ⟨3D⟩ model lines with different recipes of microturbulence for full atmosphere model at 23-km resolution.

We continue the comparison by looking at the same atmosphere with a higher resolution, 6-km resolution. Since the resolution is higher this atmosphere will have a more detailed view of the same area, as seen in the intensity plot, (Figure 2.1). For this atmosphere, we again look at the Ca II 854.2 nm line for the 3D model and the averages with different microturbulence recipes.

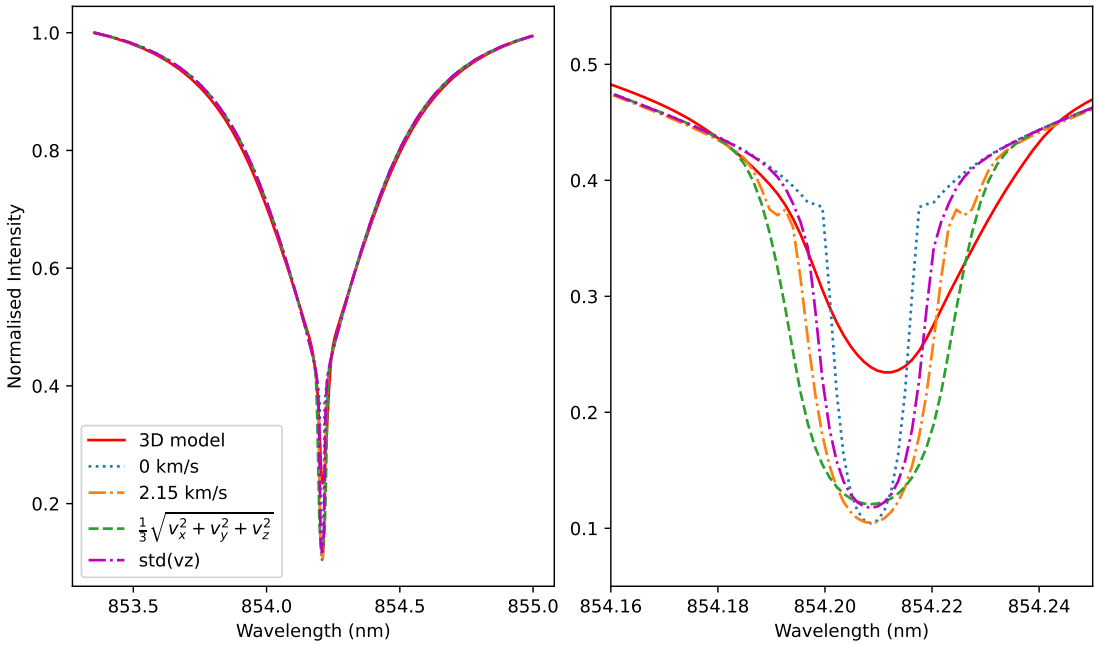

Figure 4.4: Ca II 854.2 nm disk-centre intensity for the 6-km resolution simulation. Left: full profile. Right: zoomed-in on line core

Figure 4.4 shows the Ca II 854.2 nm spectral line for the 3D model and ⟨3D⟩ with

four different microturbulence recipes. From these lines, we calculated the equivalent width to compare the averages to the three-dimensional model. Equivalent width values and deviation percentages for the lines in Figure 4.4 are in Table 4.2.

Line Profile	**W (nm)**	**Deviation from 3D model**
3D spatial average	0.304	—
0 km/s	0.299	−1.79%
2.15 km/s	0.302	−0.78%
$\frac{1}{3}\sqrt{v_x^2 + v_y^2 + v_z^2}$	0.303	−0.39%
std(v_z)	0.300	−1.33%

Table 4.2: Ca II 854.2 nm equivalent widths for 3D model line and ⟨3D⟩ model lines with different recipes of microturbulence for full atmosphere model at 6-km resolution.

We see that the equivalent widths are quite close with the maximum difference being −1.79% and the best line having a difference in equivalent width of only −0.39%. Despite this, we see in the right image of Figure 4.4 that the line cores of the ⟨3D⟩ models are not a good match to the 3D model line core. All the average model lines are stronger and wider than the 3D model line core, the equivalent width is again compensated in the wings of the line where the 3D line is stronger. We see that the trend for the higher resolution atmosphere is the same as for the same atmosphere with lower resolution, the lines are close in equivalent width, but look quite different in shape. For this higher resolution atmosphere, the equivalent width for the ⟨3D⟩ model lines is closer to the 3D model line equivalent width than for the lower resolution. When comparing the line profiles from the low resolution atmosphere in Figure 4.3 to the line profiles from the high resolution atmosphere in Figure 4.4 we see that most of the ⟨3D⟩ lines are similar in the two resolutions, the main different is the ⟨3D⟩ with the $\frac{1}{3}\sqrt{v_x^2 + v_y^2 + v_z^2}$ microturbulence recipe. This line is narrower in the high resolution than in the low resolution atmosphere, it is unclear why this line has such a large difference depending on resolution compared to the other lines.

From the line profiles for the full atmosphere, we can see that the addition of microturbulence alone does not make a ⟨3D⟩ model line a good approximation to the 3D model line, there are still large discrepancies. This means that adding microturbulence is not sufficient in making a good model. However, we want to look more closely at the different microturbulence recipes to see if they improve the model and through this see if there is a connection between the microturbulence, the discrepancies and physical parameters. To do this we look at smaller areas of the atmosphere.

4.2.2 Smaller Boxes

When looking at the smaller boxes we have many smaller atmosphere models, and we have one $\langle 3D \rangle$ model for a each box, meaning that we have many smaller models that can be put together. Through this method we can see if the smaller boxes will make the $\langle 3D \rangle$ model line a better approximation to the 3D model line. The smaller boxes allow us to see in which areas of the atmosphere the intensity of the $\langle 3D \rangle$ model is close to the intensity of the 3D model when we have added different microturbulence recipes. As mentioned the equivalent width is not always a good measure, especially if there is a possibility of small emission peaks in the line profile or irregular lines. As we make the boxes we average over smaller there is a larger possibility of different shapes for the lines, we will therefore be using the goodness of fit, to compare the lines in this case. Using the goodness of fit measure we give each box an intensity squared difference value, Γ, to see which boxes have the best fit.

First, we look at the goodness of fit for the small boxes for the low resolution version of the atmosphere. As explained for this atmosphere the small boxes will be 230 km in each horizontal direction, meaning we have 51 different boxes in x and 51 boxes in y. Each of these 2601 boxes also has an average model.

In Figure 4.5 we see the goodness of fit for each small box the 23-km per pixel resolution atmosphere. Lighter areas have higher Γ values and higher intensity differences and darker areas have lower Γ values and lower intensity differences. From these images, we see that when we have small boxes the 0 km/s microturbulence has the lowest Γ values overall. This means that when the boxes are this small it seems it is best to have no added microturbulence to the $\langle 3D \rangle$ model. A box of about 230 km in the x and y direction means that its size is less than the size of a typical granule. When the boxes are this small many of the boxes will only contain one granule and will have less velocity from the motions between granules. If microturbulence is a real motion, we would expect to see that added microturbulence to the averages improves the average also on small scale.

To look further into this we also examine the small boxes for the same atmosphere at a higher resolution. The higher resolution has more detail and can sometimes contain important changes in the atmosphere that the lower resolution does not include. As mentioned we have roughly the same physical size in the different resolutions, for the small boxes we have about 228 km in x and y, and therefore have 53 boxes in each horizontal direction.

Figure 4.6 shows the goodness of fit for small boxes made from the high-resolution atmosphere. Here we see that the upper images have more areas where the difference is large than the lower images, it seems from these images that with this atmosphere resolution the best microturbulence addition is the standard deviation of the velocity in the z-direction and the worst is if we add no microturbulence. We see from this figure that overall the goodness of fit is worse in more boxes for this high resolution than for the lower resolution we saw in Figure 4.5, this seems to be the case for all microturbulence values. Generally, a higher resolution means more detail, and this can mean that there are more changes in each of the boxes. If each box has more changes in intensity,

and perhaps more sudden changes, the ⟨3D⟩ will have more trouble representing the atmosphere accurately.

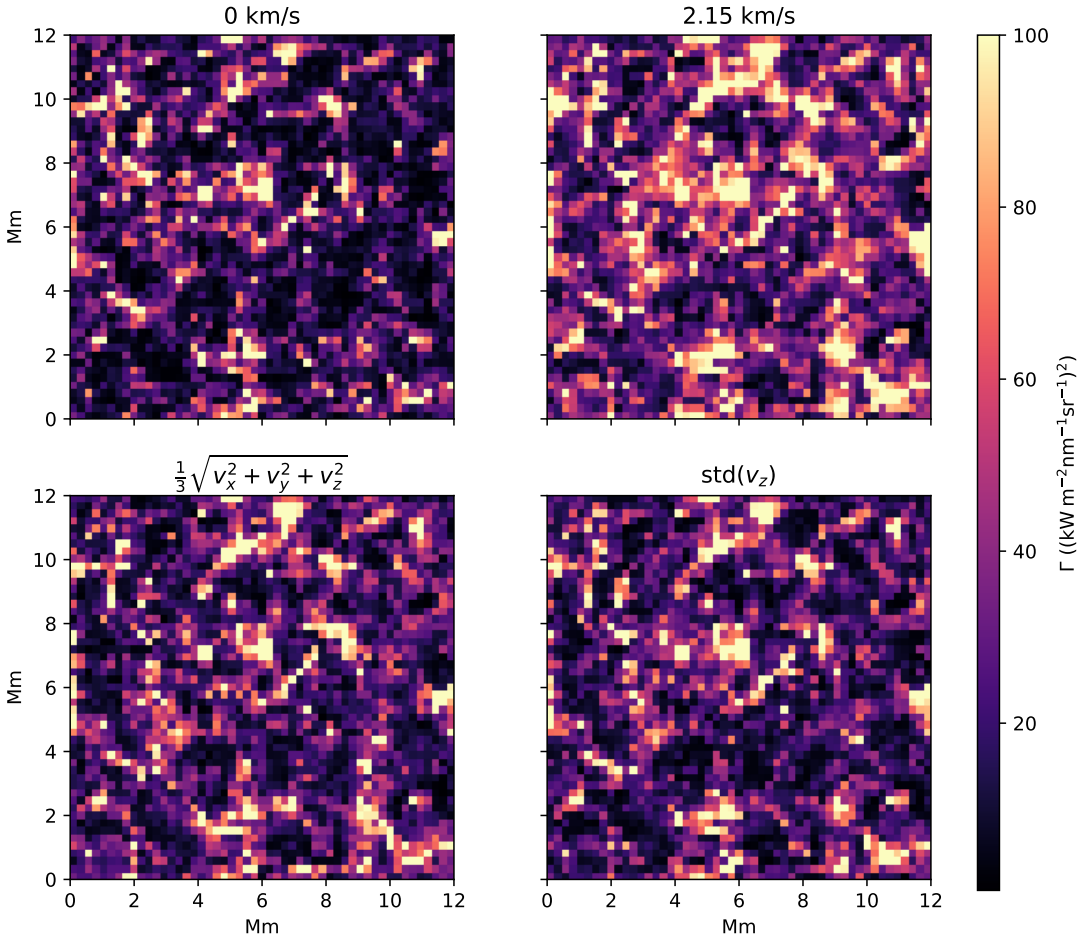

Figure 4.5: Goodness of fit map for the 23-km resolution atmosphere split into 51 boxes of approximately 230 km in each horizontal direction. Intensity squared difference (Γ) between the Ca II 854.2 nm line for the 3D model and the ⟨3D⟩ models.

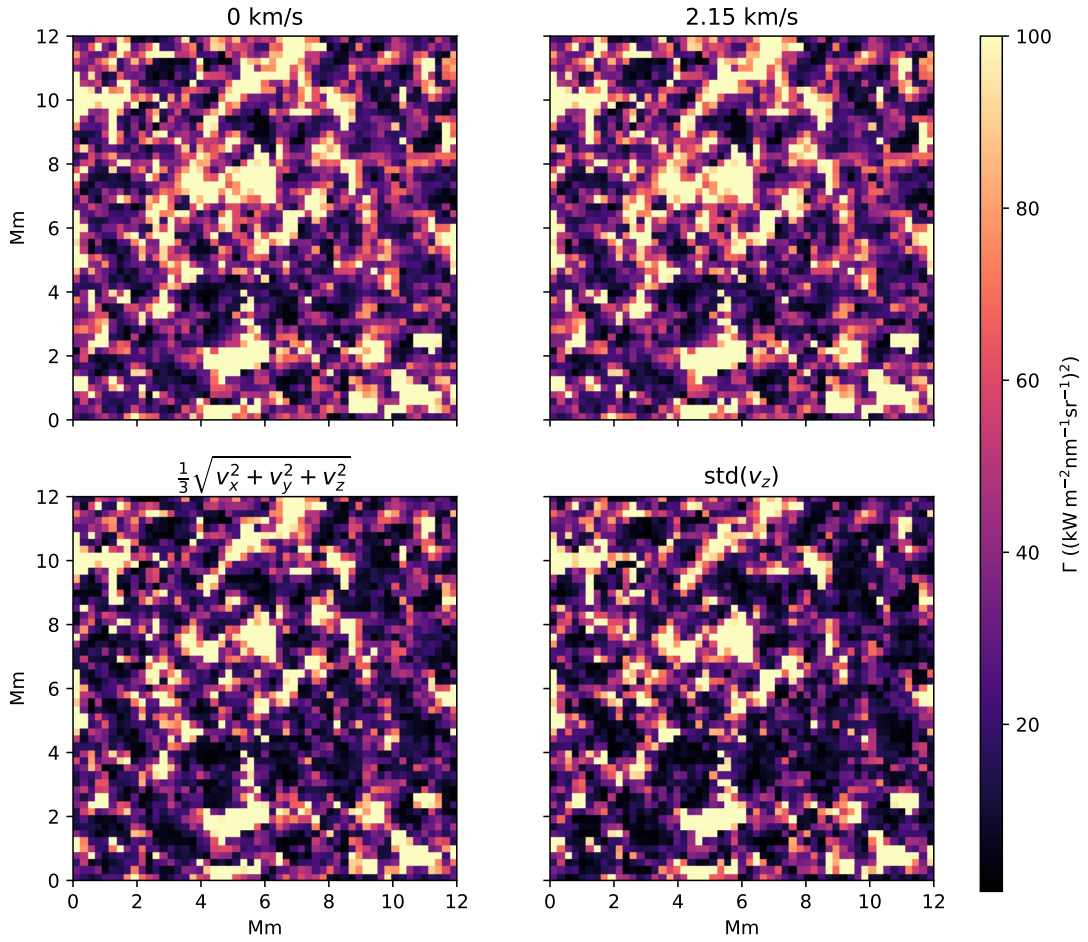

Figure 4.6: Goodness of fit map for the 6-km resolution of the atmosphere split into 53 boxes of approximately 228 km in each horizontal direction. Intensity squared difference (Γ) between the Ca II 854.2 nm line for the 3D model and the $\langle$3D$\rangle$ models.

We have seen that for the small boxes the average is better without any addition of microturbulence when looking at low resolution and best with microturbulence for high resolution. There is thus a difference in the results based on resolution. As we hypothesise that the higher resolution atmosphere has larger Γ values due to more motions we see that the addition of microturbulence lowers this Γ value and makes the fit better. We will explore why this is the case when exploring the roots of microturbulence and the precision of the averaging method. However, to be sure that the motions creating the microturbulence are not overseen due to the box being smaller than the average granule, we also look at the Γ maps for the larger boxes. First, we look at the

1150km boxes in the low-resolution atmosphere. There are 100 of these boxes and thus also 100 averages for this size box.

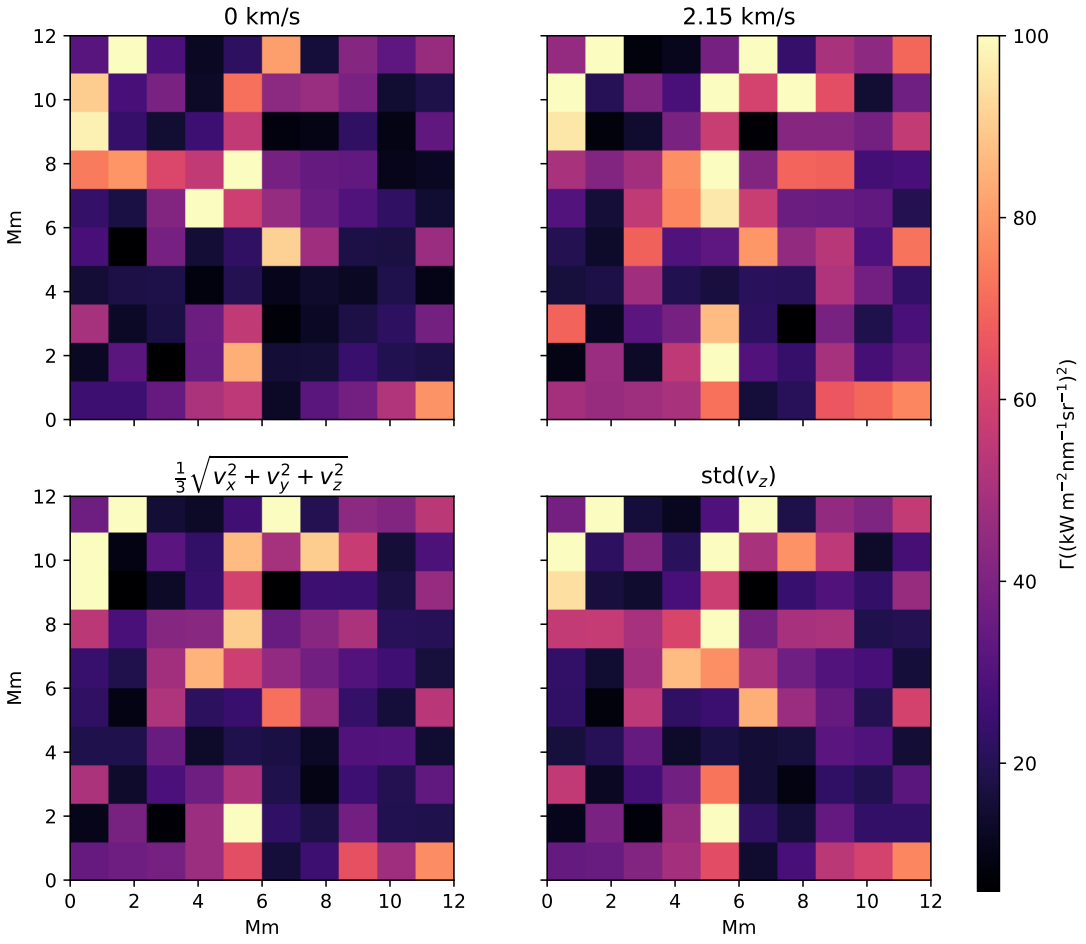

Figure 4.7: Goodness of fit map for the 23-km resolution of the atmosphere split into 10 boxes of approximately 1150 km in each horizontal direction. Intensity squared difference (Γ) between the Ca II 854.2 nm line for the 3D model and the $\langle$3D$\rangle$ models.

In Figure 4.7 we see the goodness of fit of the Ca II 854.2 cm line in the 23-resolution atmosphere for the larger boxes. Compared to Fig. 4.5 we now see that there is no longer a much lower Γ value when we have no microturbulence. It seems that no microturbulence is still better than the constant microturbulence, but that using the standard deviation of v_z or $\frac{1}{3}\sqrt{v_x^2+v_y^2+v_z^2}$ are as good if not slightly better in some

areas. When we use this size box with 23-resolution we get a physical size of 1150 km in x and y-direction for each box, so we have a larger area and expect more motions within each box. Again, we look at the high-resolution atmosphere as well. Here we have boxes roughly the same size, 1152 km in each direction, and again 100 boxes with 100 average models.

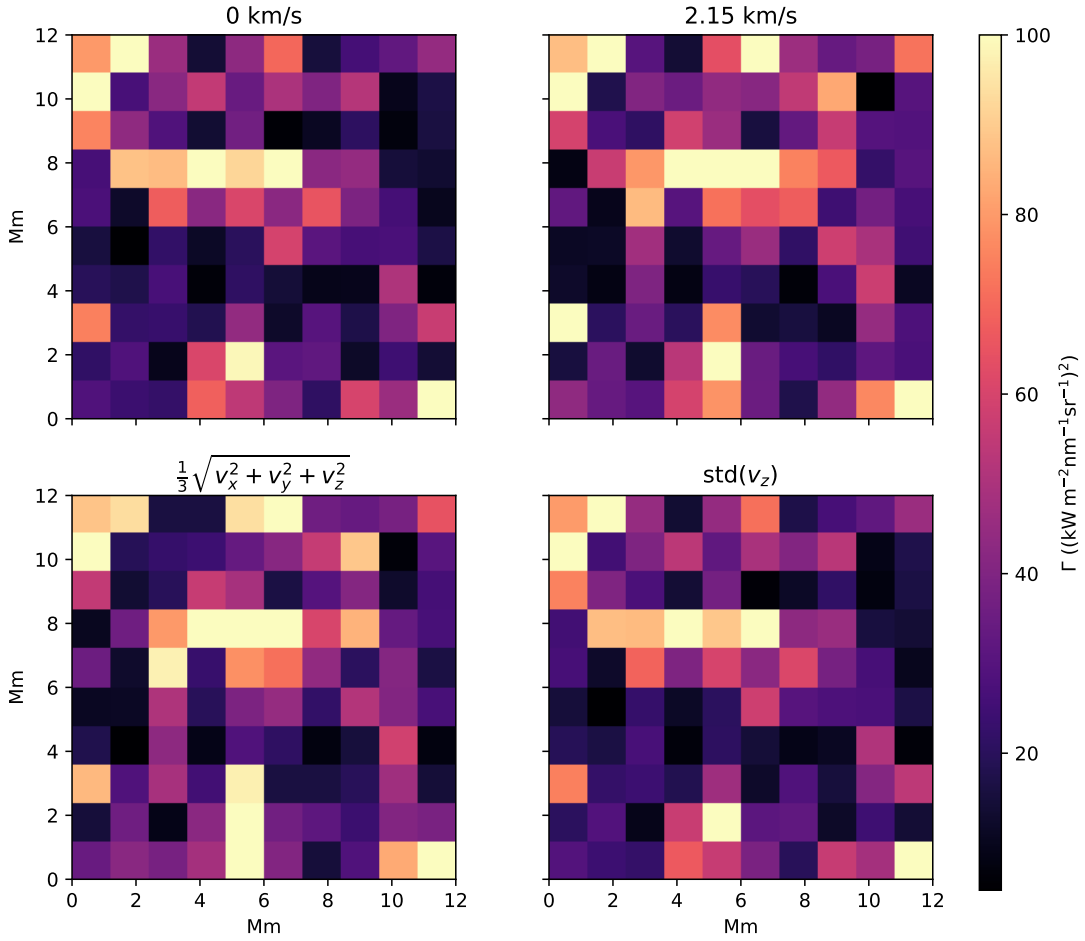

Figure 4.8: Goodness of fit map for the 6-km resolution of the atmosphere split into 10 boxes of approximately 1150 km in each horizontal direction. Intensity squared difference (Γ) between the Ca II 854.2 nm line for the 3D model and the ⟨3D⟩ models.

As seen in Figure 4.6, Figure 4.8 also shows that the Γ value is higher for the high-resolution atmosphere than for the low-resolution atmosphere regardless of the microturbulence recipe. Again this can be explained by the more detailed changes in

intensity that are more difficult to represent in an average model. Figure 4.8 shows that the difference in squared intensity in the different microturbulence recipes is not very large, although the 0 km/s and the standard deviance seem to give a difference that is slightly smaller than the other microturbulence recipes. We have seen in both resolutions that when we make the boxes larger the addition of microturbulence is almost insignificant.

When looking at the line profiles and the Γ values for the different atmospheres we see that for the smallest boxes Γ is smaller when no microturbulence is added, for the larger boxes Γ is almost the same regardless of microturbulence and when looking at the whole atmosphere the equivalent width is best when there is microturbulence added. It seems that the larger area we average over the more beneficial the addition of microturbulence is to the fit, this might indicate that the microturbulence is not a real motion but rather a factor that compensates for simplification in the average. We also see that the microturbulence does not make the $\langle 3D \rangle$ lines good approximations of the 3D line in shape and strength.

4.3 Roots of Microturbulence

We have seen from the comparison of the different microturbulence recipes that the addition of microturbulence does not make a big improvement, and in the smallest boxes, the addition of microturbulence generally makes the model worse. As we have seen that if we split the atmosphere into smaller boxes the atmospheres with added microturbulence are worse than the atmospheres without we can assume that the size of the atmosphere we look at will affect whether microturbulence is a good addition to the model or not. In the smallest of the boxes, we see that there is no benefit to adding a microturbulence to improve the fit in most cases this will make the model worse, in the medium boxes there seems to be little to no difference in the deviation from the 3D model if we add microturbulence, when we looked at the whole atmosphere however we see that the line for the $\langle 3D \rangle$ model is closer to the 3D model with the addition of microturbulence. This might be a result of the way we average, if we average a larger area the smaller motions will most likely cancel each other and a $\langle 3D \rangle$ will then be closer to the 3D model. In the smaller boxes, however, the lines are more influenced by each column and thus one high value of a variable can change the $\langle 3D \rangle$ model even though it will not have a large effect on the 3D model. Some of the effects that can influence the lines in the smaller boxes can cause asymmetry in the line which can not be compensated for with the addition of microturbulence. If we look at the lines in two of the boxes in the low-resolution atmosphere we can see how these lines for the small boxes are quite different from the lines in a larger atmosphere area. Here we look at two of the smaller boxes for the low-resolution atmosphere, one where Γ is low and one where Γ is high.

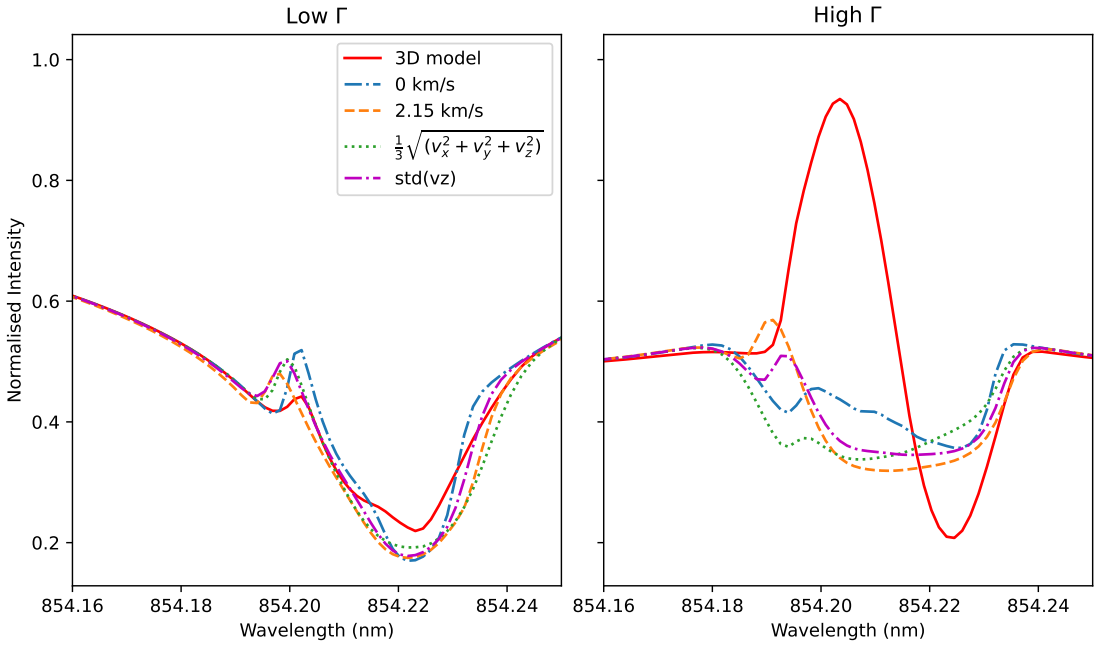

Figure 4.9: Line profiles zoomed-in on the line core from two of the 230 km boxes from the 23-km resolution atmosphere. Low Γ box (box with midpoint at 575 km in x and 115 km in y direction) and high Γ box (box with midpoint at 2415 km in x and 805 in y direction).

When comparing the lines for the smaller boxes in Figure 4.9 to the lines we have seen for the full low-resolution atmosphere in Figure 4.3, we see that these lines for the smaller boxes have much more asymmetry. Here we have chosen to look at one of the boxes that has a low Γ value (low difference in intensity) and one of the boxes that has a high Γ value (high difference in intensity). We see for both boxes that the shape of the one-dimensional averages are more irregular than we saw when we looked at the full atmosphere, but we also see that for the box with a high Γ there are asymmetries in the shape and a combination of emission and absorption. Such a line is much more difficult to achieve when we average because the variables are averaged and therefore the intensity calculations are not the same. In this line with a high Γ we have a high difference in intensity between the 3D model line and the ⟨3D⟩ model lines, which is also reflected in the shape of the line.

When splitting the atmosphere into boxes we saw that for all the different microturbulence recipes the Γ values are largest in the same areas. When we have the additional microturbulence we get larger Γ in some of the boxes, but the general trend is the same as for the averages where no microturbulence is added. Since this seems to be the case for all the different situations we looked at, a reasonable assumption is that the main difference between the ⟨3D⟩ model and the 3D model lines comes from the averaging itself and not from the addition of a microturbulence factor. Therefore, we want to firstly focus on where the averaging difference comes from. This is important

because the splitting of the atmosphere into small boxes showed that the addition of microturbulence at a small scale exacerbates the difference we get from averaging.

4.3.1 Effect of Averaging

We explore where this averaging difference comes from by looking at the individual variables that contribute to the shape of the spectral lines. Thus, we will look at how the temperature and line of sight velocity differ between the $\langle 3D \rangle$ model and the 3D model. In Fig. 4.10 we see the line of sight velocity as a function of the optical depth for two different small boxes in the low-resolution atmosphere. In one of the boxes, we have a low Γ value and in the other, we have a high Γ value, we have chosen one with a low and one with a high Γ value so that we can look at the differences in the z-velocity as the Γ is higher. These are the same boxes as we looked at for the line profile in Figure 4.9. For each of the boxes, the line of sight velocity of the average model is plotted in addition to the line of sight velocity for all the columns of the 3D model that make up the box we are looking at.

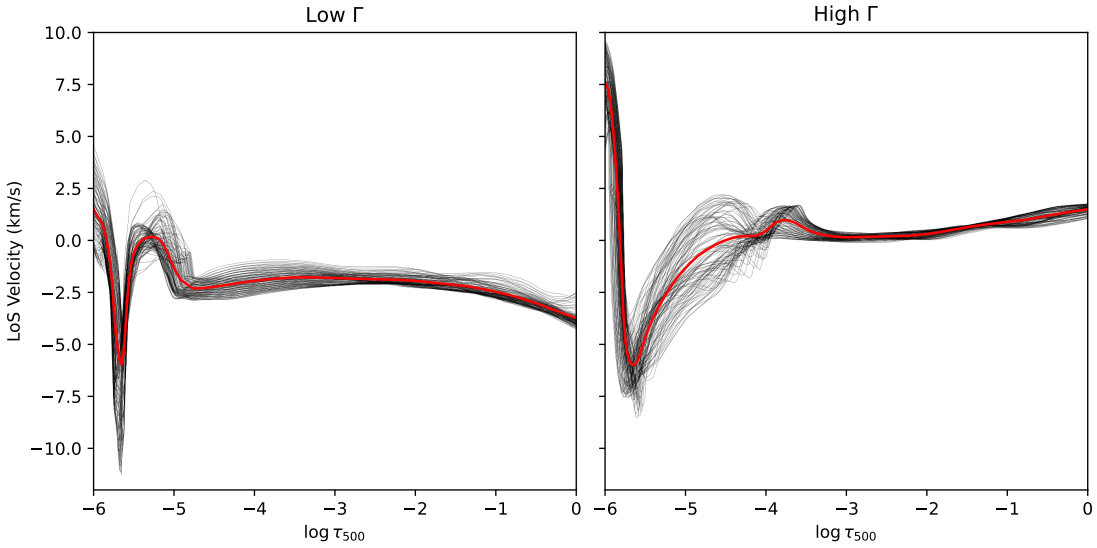

Figure 4.10: Line of sight velocity as a function of the logarithm of optical depth for two different small boxes in 23-km resolution atmosphere. Red line is the $\langle 3D \rangle$ model, black lines are each column of 3D model

These images show that the box with the highest Γ has a larger spread in line of sight velocity in the 3D model columns than the box with the lower Γ. We see that in the range from $\log(\tau_{500}) = -6$ to $\log(\tau_{500}) = -3.5$ the high Γ box the spread in values is much larger, this is corresponding to the height where Ca II 854.2 nm line is formed. This can explain the higher Γ value as this larger spread makes it more difficult for the average to represent the full 3D model.

In the images in Figure 4.5 and Figure 4.6, we saw that the high-resolution atmo-

sphere had overall higher Γ values than the low-resolution atmosphere. As we believe these higher values stem from more changes in each box due to the increased resolution we also want to look at the line of sight velocity for the same boxes in the higher resolution atmosphere. For a higher resolution atmosphere, there is a larger number of pixels for the same physical area, and thus we also have a larger number of columns when we plot the variables here. We expect there to be a larger spread in the columns of the 3D model in higher resolution than in lower resolution. Here we are looking at the same boxes for high resolution as we did for the lower resolution in order to compare the boxes with each other.

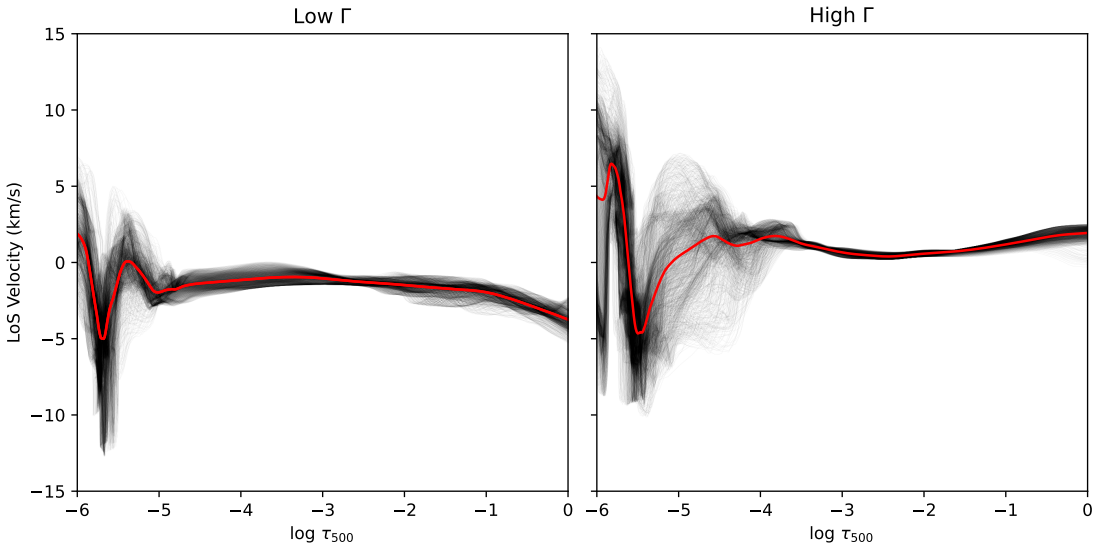

Figure 4.11: Line of sight velocity as a function of the logarithm of optical depth for two different small boxes in 6-km resolution atmosphere. Red line is the ⟨3D⟩ model, black lines are each column of 3D model

When comparing the line of sight velocity difference between the columns of the 3D model and the ⟨3D⟩ model in the two different resolutions we see that the higher resolution does indeed have a larger spread. As mentioned there are more columns in the higher resolution, but we also see that there is a larger difference between the highest and lowest values. When there is a larger spread in the columns that the ⟨3D⟩ model has to average the model has a more difficult time averaging. Since the columns all are black lines the areas in the graph with a higher density, darker areas, are where most of the columns lie. We see in Figure 4.11 that around the $\log(\tau_{500}) = -4$ the ⟨3D⟩ deviates from the value with the highest density of columns. This is because there are columns that have lower values that make the average lower than the mode value.

We also want to look at the temperature similarly. For both the high and low resolution we look at a box where the Γ value is low and a box where the Γ value is high. For the temperature, we look at the same boxes as we did for the line of sight velocity. We again expect the average to be worse in the box with the higher Γ and also

be worse in the higher resolution.

In Figure 4.12 we see that also for the temperature the columns are more spread for the box with higher Γ and less spread in the box with lower Γ. We again want to compare this to the high-resolution atmosphere and look at the same boxes as we did for the lower resolution atmosphere.

Figure 4.13 shows the temperature as a function of optical depth for the 3D model columns and the average model for the high-resolution simulation. Here we see, as for the lower resolution, that the box with higher Γ has the largest spread in the temperature for the different columns. This makes it more difficult to get a good average, making the average a worse approximation to more columns and thus the line profile for the average model deviates more from the 3D model line profile.

Overall, it seems that when we make an average model of the solar atmosphere we will get spectral lines that are not a very good fit to spectral lines we get when using a three-dimensional model. Moreover, it seems that the difference between a ⟨3D⟩ model and a 3D model is exacerbated rather than diminished when we add a microturbulence factor to the model. When looking at these atmospheres, especially when they are broken down into smaller parts, we get the idea that the differences in the averaged models are mostly from the averaging itself. In addition, it seems that microturbulence does not, in general, make up for the simplification of the model. Since we see that there is a relation between Γ and the physical parameters temperature and line of sight velocity, we can surmise that the microturbulence is not an existing and missing motion, but rather a difference in the models that is created from averaging and oversimplifying a complicated area of the solar atmosphere.

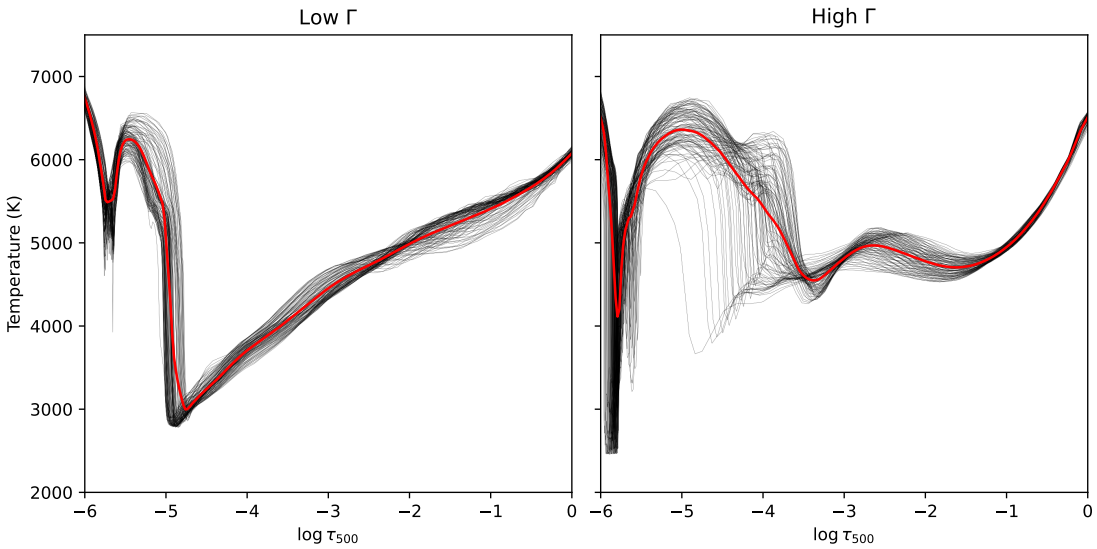

Figure 4.12: Temperature as a function of the logarithm of optical depth for two different small boxes in 23-km resolution atmosphere. Red line is the ⟨3D⟩ model, black lines are each column of 3D model

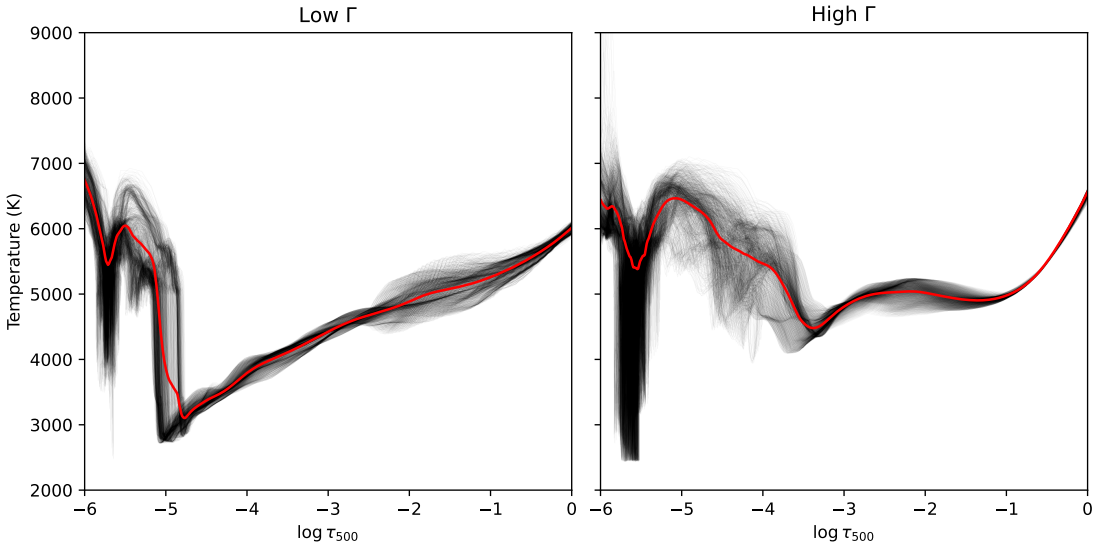

Figure 4.13: Temperature as a function of the logarithm of optical depth for two different small boxes in 6-km resolution atmosphere. Red line is the ⟨3D⟩ model, black lines are each column of 3D model

4.3.2 Physical Parameters in Different Boxes

To look more closely at the relationship between the difference in intensity and the temperature and line of sight velocity we look at the variables at the height around where the Ca II 854.2 nm line is formed, and see from the figures that there is a large difference between the 3D model columns and the ⟨3D⟩ model for both temperature and line of sight velocity at a height of $\log \tau_{500} = -5$. If we look at the mean line of sight velocity and the mean temperature for each box at this height we can try to compare this to the difference we get for the intensity. We will be looking at the smaller boxes because the Γ map created from these is more easily readable than the Γ map from the larger boxes. We saw in Figure 4.5 that the differences were in approximately the same areas for all the microturbulence additions, the only difference seems to be larger Γ values for the microturbulence additions, therefore we will be comparing the variables to the microturbulence addition that gave the largest Γ values to see if there is any correlation. Since we see in both resolutions that the average model deviates from the columns and the columns have a large spread at $\log_{10} \tau_{500} = -5$ we will only be looking at the mean parameters in relation to the low resolution atmosphere.

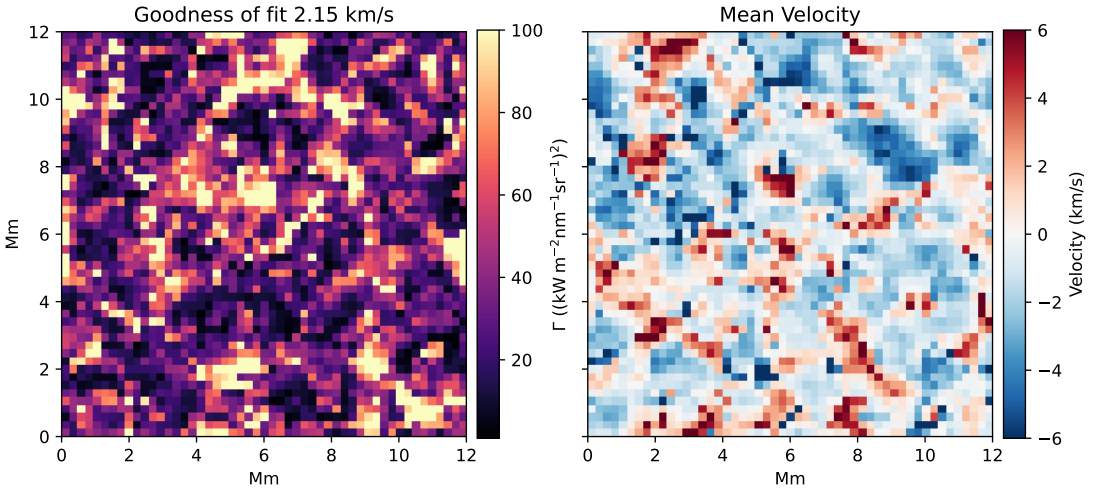

Figure 4.14: Right: Intensity squared error, Γ, for small boxes in 23-km resolution atmosphere with 2.15 km s^{-1} additional microturbulence. Left: Mean velocity at $\log_{10}\tau_{500} = -5$ for each of the small boxes.

From Figure 4.14, we see the Γ map for one microturbulence recipe and the mean velocity map, here the mean velocity is the mean velocity in x- and y-direction at the height where $\log_{10}\tau_{500} = -5$. There seems to be a relation between the higher Γ areas and the areas that have a high mean velocity in some areas, but in other areas where the Γ is large, the velocity is not large. Since there is some relation the value of the mean velocity will most likely influence the Γ, but this alone cannot explain the difference.

We also look at the relation between the Γ values and the mean temperature. Again the temperature for each box is calculated to be the average temperature in x-and y-direction at the height where $\log_{10}\tau_{500} = -5$ because this is a height where we in 4.12 saw a large spread in the 3D model temperature columns. This is also within the region of formation for the line core of this line.

Figure 4.15 we see the Γ map of 2.15 km s^{-1} microturbulence and the mean temperature map for the same boxes. This mean temperature value was calculated by taking the mean of the temperature values from the 3D model in each box at the height where $\log_{10}\tau_{500} = -5$. It shows as we saw for the line of sight velocity, that the Γ map seems to have some of the same shapes as we see in the mean temperature image, but that all the differences are not related to the temperature. It seems that in areas with high temperature there is in many cases also higher Γ, which could be explained from the Doppler width as this is a term with temperature and microturbulence and if the already high temperature is combined with additional microturbulence we will have a line that is broader than the line from the 3D model. From these images, it seems that both the line of sight velocity and the temperature play a part in creating the averaging

differences and the additional difference that we get in the atmospheres where we have added microturbulence.

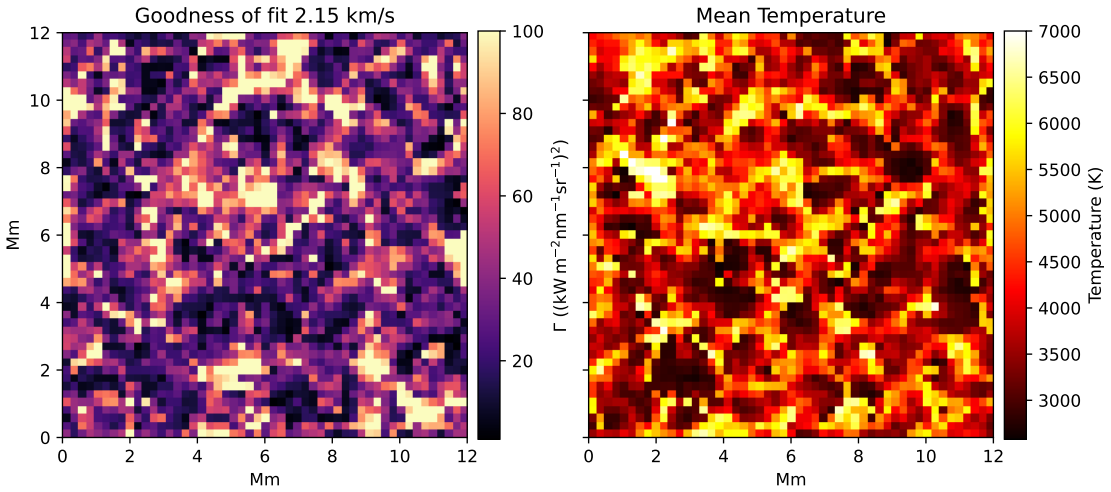

Figure 4.15: Right: Intensity squared error, Γ, for small boxes in 23-km resolution atmosphere with 2.15 km s^{-1} additional microturbulence. Left: Mean temperature at $\log_{10} \tau_{500} = -5$ for each of the small boxes.

Chapter 5

Conclusion and Future Work

5.1 Conclusion

Overall, we can see that the improvement from the addition of microturbulence in the Ca II 854.2 nm line from a $\langle 3D \rangle$ model is very limited when comparing it to the full 3D calculations. It is not necessarily a good parameter to use in an attempt to improve this $\langle 3D \rangle$ model. We have seen that when we have a $\langle 3D \rangle$ model averaged over a large area of the atmosphere the addition of microturbulence to the one-dimensional model can improve the line profile fit by giving the line an equivalent width that is closer to the equivalent width of the 3D line from the model of the same atmosphere area. We saw that the equivalent width of the $\langle 3D \rangle$ model was closest to that of the 3D model in both resolution atmospheres with the addition of $\frac{1}{3}\sqrt{v_x^2 + v_y^2 + v_z^y}$ as the microturbulence parameter. However, we also saw that despite the improvement in the equivalent width compared to the 3D model, the shape of the $\langle 3D \rangle$ line profiles with microturbulence is still not a good estimate of the shape of the 3D line profile. The spectral lines from the $\langle 3D \rangle$ models are generally stronger and broader near the line core. When splitting the atmosphere into boxes and looking at smaller areas we found that the addition of microturbulence increased the Γ of the line rather than decreased it for the smallest boxes. This is likely because the average will be more affected by small scale motions when we look at areas of this size, the average model itself will create a bad estimate and the addition of microturbulence will then only exacerbate the difference that is already present in the average. We saw in the smallest boxes with higher resolution that the addition of microturbulence did reduce Γ in some areas. Thus, we had slightly different results depending on the spatial resolution we used for the model. For low resolution it did not improve the $\langle 3D \rangle$ models, but for high resolution it did. However, when looking at how the averages are made compared to the 3D model columns it seems that there is a correlation between the Γ values and the averaging. The higher resolution has larger spread in values for the parameters and more changes in each box will thus be more difficult to make a good average of. Since the $\langle 3D \rangle$ line profile is a less good fit for the higher resolution atmosphere the model will benefit from the addition of microturbulence as a broadening parameter. In the bigger boxes the microturbulence

addition did not make the ⟨3D⟩ line profiles better or worse in general. Here we saw that the addition of microturbulence did not have a large effect on the Γ value. We thus have different results for the different sizes of the atmosphere area. At a larger scale, the averages are smoothed over larger areas and thus the microturbulence can improve the Γ and W values, but not the shape of the line. While at the smaller scale the microturbulence does not overall improve the ⟨3D⟩ line profile.

We found no clear correlation between either temperature or velocity and the Γ value that in itself can explain the need for microturbulence. However the Γ value seems to have some relation both to temperature and velocity. We saw the that high velocity areas correspond somewhat to the areas with high Γ values. In addition, we saw that high temperature also seem linked to high Γ value. As these parameters both contribute to the spectral line and temperature is also connected to the broadening it seems reasonable that there is a correlation. If high temperature and high velocity cause larger differences between the models this likely stems from the high mean values being more difficult to capture in an average.

Since we see that the main difference between the lines on a small scale is from the averaging method and microturbulence only improves the lines on a large scale we presume that microturbulence is only a parameter that is added due to the lack of a good model. If microturbulence were to be a real motion we would expect an improvement on the line profiles also on the smaller scales we have looked at. We also saw that the resolution and the size of the boxes influenced which microturbulence recipe gives the lowest difference between the 3D model and the ⟨3D⟩ models. This is also an indication that microturbulence is not a real motion, but rather a tuning parameter that compensates for the loss of information in a ⟨3D⟩ model compared to a 3D model. We have also found that from the four microturbulence recipes the one that improves the model the most in the cases where we see improvement in equivalent width or Γ is $\frac{1}{3}\sqrt{v_x^2 + v_y^2 + v_z^2}$ which is the recipe suggested by Uitenbroek & Criscuoli (2011). This is a microturbulence value that changes with height, which is not often included for this line and is different from the microturbulence used for NLTE chromospheric lines in Quintero Noda et al. (2016) and de la Cruz Rodríguez et al. (2012).

5.2 Future Work

We looked at the Γ maps for the different ⟨3D⟩ models, and subsequently at the root of the main intensity differences. As mentioned, we saw a difference in the results when looking at the different resolutions for the smallest boxes. This can be a result of the averaging method, but this difference in Γ between the models should be explored further.

In addition, the main takeaway from this project is that the addition of microturbulence does not make a ⟨3D⟩ model a good model for the solar chromosphere. Therefore it would be beneficial in the future to look at different averaging methods for the ⟨3D⟩ model or perhaps explore the model with the addition of macroturbulence as well or other parameters which could potentially explain the difference in the profile shapes

near the line core.

Bibliography

Asplund, M. 2005, ARAA, 43, 481, doi: 10.1146/annurev.astro.42.053102.134001

Beck, C., Choudhary, D. P., Rezaei, R., & Louis, R. E. 2015, ApJ, 798, 100, doi: 10.1088/0004-637X/798/2/100

Carlsson, M., De Pontieu, B., & Hansteen, V. H. 2019, ARAA, 57, 189, doi: 10.1146/annurev-astro-081817-052044

da Silva Santos, J. M., de la Cruz Rodríguez, J., Leenaarts, J., et al. 2020, A&A, 634, A56, doi: 10.1051/0004-6361/201937117

de la Cruz Rodríguez, J., Socas-Navarro, H., Carlsson, M., & Leenaarts, J. 2012, A&A, 543, A34, doi: 10.1051/0004-6361/201218825

Edvardsson, B., Andersen, J., Gustafsson, B., et al. 1993, A&A, 275, 101

Gudiksen, B. V., Carlsson, M., Hansteen, V. H., et al. 2011, A&A, 531, doi: 10.1051/0004-6361/201116520

Gustafsson, B., Edvardsson, B., Eriksson, K., et al. 2008, A&A, 486, 951, doi: 10.1051/0004-6361:200809724

Leenaarts, J., Carlsson, M., Hansteen, V., & Rouppe van der Voort, L. 2009, AJ, 694, L128. https://arxiv.org/abs/0903.0791

Magain, P. 1984, A&A, 134, 189

Magic, Z., Collet, R., Hayek, W., & Asplund, M. 2013, A&A, 560, A8, doi: 10.1051/0004-6361/201322252

Moe, T. E., Pereira, T. M. D., & Carlsson, M. 2022, arXiv e-prints, arXiv:2204.08849. https://arxiv.org/abs/2204.08849

Mucciarelli, A. 2011, A&A, 528, A44, doi: 10.1051/0004-6361/201015814

Pereira, T. M. D., & Uitenbroek, H. 2015, A&A, 574, A3, doi: 10.1051/0004-6361/201424785

Quintero Noda, C., Shimizu, T., de la Cruz Rodríguez, J., et al. 2016, MNRAS, 459, 3363, doi: 10.1093/mnras/stw867

Ruiz Cobo, B., & del Toro Iniesta, J. C. 1992, ApJ, 398, 375, doi: 10.1086/171862

Rutten, R. J. 2003, Radiative Transfer in Stellar Atmospheres

Sainz Dalda, A., de la Cruz Rodríguez, J., De Pontieu, B., & Gošić, M. 2019, ApJL, 875, L18, doi: 10.3847/2041-8213/ab15d9

Socas-Navarro, H. 2015, A&A, 577, A25, doi: 10.1051/0004-6361/201425049

Steffen, M., Ludwig, H. G., & Caffau, E. 2009, Mem. Soc. Astron. Italiana, 80, 731. https://arxiv.org/abs/0909.2831

Takeda, Y. 2022, Solar Phys., 297, 4, doi: 10.1007/s11207-021-01931-0

Uitenbroek, H. 2001, AJ, 557, 389, doi: 10.1086/321659

Uitenbroek, H., & Criscuoli, S. 2011, AJ, 736, 69, doi: 10.1088/0004-637X/736/1/69